A review of dynamic recrystallization phenomena in metallic materials

K. Huang *, R.E. Logé

Thermomechanical Metallurgy Laboratory – PX Group Chair, Ecole Polytechnique Fédérale de Lausanne (EPFL),CH-2002, Neuchâtel, Switzerland

HIGHLIGHTS

- Three types of dynamic recrystallization processes occurring during hot deformation are reviewed.
- The mechanisms of these three types of dynamic recrystallization processes are discussed in detail.
- Physically based numerical models for all the three dynamic recrystallization process are reviewed.
- Topics for further investigation on dynamic recrystallization are recommended.

GRAPHICAL ABSTRACT
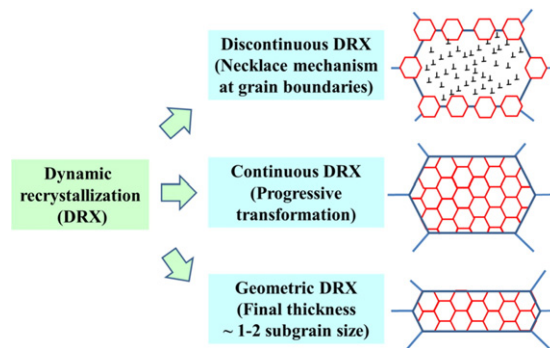
ARTICLE INFO

ABSTRACT

The dynamic recrystallization (DRX) phenomena occurring in different thermo-mechanical processing (TMP) conditions for various metallic materials are reviewed. Several types of DRX are described: discontinuous dynamic recrystallization (DDRX), continuous dynamic recrystallization (CDRX) and geometric dynamic recrystallization (GDRX). The terminologies used in this field are summarized, together with the key factors influencing the DRX processes including stacking fault energy, initial grain size, TMP conditions and second-phase particles. Both standard and advanced experimental techniques used to characterize DRX processes are examined. The focus is placed on the mechanisms of these three types of DRX, and the related numerical models.

© 2016 Elsevier Ltd. All rights reserved.

Contents

---

* Corresponding author.
  E-mail addresses: ke.huang@epfl.ch, huangke0729@hotmail.com (K. Huang).

1. Introduction

Most of the metallic parts have been, during their processing cycle, subjected to hot deformation, during which dynamic recrystallization (DRX) often takes place. The final microstructure and mechanical properties of the alloys are largely determined by the recrystallization and related annealing phenomena, and the research on recrystallization can date back to 150 year ago [1]. The fast development of the DRX theory from 1960s was summarized by McQueen in 2004 [2]. A lot of important factors can have a significant effect on DRX, these include the stacking fault energy (SFE), the thermo-mechanical processing (TMP) conditions, the initial grain size, chemistry and microchemistry of the material in terms of solute level and second phase particles etc., which is also the reason why a vast amount of related works can be found in the literature.

During hot deformation, discontinuous dynamic recrystallization (DDRX) is frequently observed for low SFE materials, where nucleation of new strain-free grains occurs and these grains grow at the expense of regions full of dislocations. Cell or subgrain structures with low angle grain boundaries (LAGBs) are formed during deformation for materials with high SFE due to the efficient dynamic recovery, they progressively evolve into high angle grain boundaries (HAGBs) at larger deformations, a process which is known as continuous dynamic recrystallization (CDRX) [1]. Besides DDRX and CDRX, another relatively new concept of geometric dynamic recrystallization (GDRX) was also observed on deforming aluminium to large strains at elevated temperatures. In this

case, the deformed grains become elongated with local serrations but remain distinguishable during deformation to large strains unless their thickness is below 1–2 subgrain size, at which time the developed serrations become pinched off and equiaxed grains with HAGBs are formed. Substantial grain refinement is thus obtained through the grain elongation and thinning. Numerical models are developed for these three types of DRX, most of them are focused on DDRX [3], with sparse models on CDRX [4] and mostly unexploited GDRX models [5].

It should be noted that there is no strict dividing line between these three types of behaviors. For example, CDRX was observed during rolling of fine-grained 304 austenitic stainless steel which is of low SFE [6], DDRX was reported for high SFE high purity Al [7], CDRX and DDRX can even co-exist during hot working of Mg—3Al—1Zn [8] or duplex stainless steel [9]. When designing new alloys, the addition of alloying elements to the base material may modify its SFE [10] and thus change the recrystallization mode. Even for the same material, changing the TMP conditions [11] or initial grain size [12] can also lead to the transition from DDRX to CDRX. Meanwhile, CDRX and GDRX can also operate concurrently, e.g., in Zircaloy-4 [13]. Due to the increasing requirements on the formability of the metallic parts, products which were previously formed at room temperature, where DRX is generally irrelevant, are now frequently processed at warm or hot temperatures [14,15]. It is not easy to simply identify which type of the three DRX processes is operating at certain TMP conditions since they share some similarities and can take place concurrently and/or transitionally. There is actually also a hot debate between researchers

within the recrystallization field on whether CDRX or GDRX should be responsible for the grain refinement of aluminium [16], the core issue is whether the HAGBs observed after large deformation are transformed from LAGBs, microshear/deformation bands, or original HAGBs.

The recrystallization phenomenon in general was reviewed in 1997 by the top experts in this area [17], since then the EBSD technique, which can provide invaluable information on the evolution of the crystallographic orientations and facilitates the understanding of different DRX processes, has been widely spread. CDRX and DDRX were recently reviewed in an excellent and extensive review paper [18], however, GDRX was not covered and the related DRX numerical models were only briefly described. The comparison of the three types of DRX processes was only occasionally mentioned in a few articles [19–21]. This short review paper covers seminal basic works as well as very recent contributions to all the three DRX processes. It differs from the above mentioned review papers since it updates key aspects on DRX from affecting factors, characterization methods to mechanisms and numerical models.

The main objective of this paper is to provide a short review of the different types of DRX observed during *hot deformation* for different types of metallic alloys, i.e., DDRX, CDRX and GDRX. The review presented is intended to equip the beginners in metallurgy with a concise insight into the DRX phenomenon. For more details on this topic, the interested readers are referred to the classic textbook on recrystallization [1] and the two excellent but longer review papers [17,18]. In Section 2, the terminologies used in this field are firstly summarized, together with the key factors influencing the DRX processes, as well as the corresponding characterization methods. The transitions between the various types of DRX processes are only briefly discussed due to the lack of literature data. From Sections 3 to 5, more details on the three types of DRX are given, including their mechanisms and related numerical models. Finally, in Section 6, further studies within the DRX field are suggested.

2. Dynamic recrystallization

2.1. Terminology

There are different phenomenological categories of recrystallization processes, many of them are interconnected and the borderlines between them are often unclear. It is beneficial to recall all these processes,
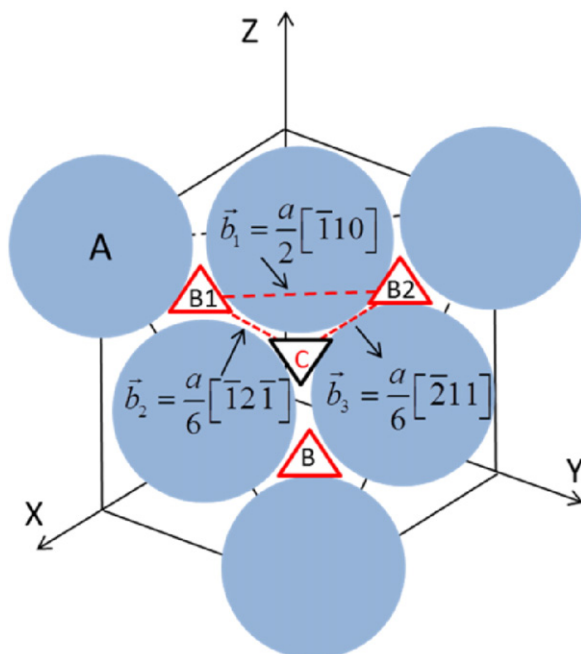

Fig. 1. Close-packed plane in an FCC metal.

even though some of them will not be covered in this review work. In addition, there are also some terminologies in recrystallization field which are worth mentioning before going into the details of DRX.

Defects like dislocations and interfaces increase during deformation which makes the material thermodynamically unstable. When deforming metal at elevated temperatures, thermally activated processes tend to remove theses defects in order to reduce the free energy of the system. The microstructure and also the properties can be partially restored to their original values before deformation by recovery through annihilation and rearrangement of dislocations. Recovery generally brings relatively homogeneous microstructural changes and it generally does not involve the migration of HAGBs between the deformed grains [17]. Similar recovery processes may take place during annealing or during deformation, which are known as static recovery (SRV) and dynamic recovery (DRV), respectively.

The "formation of a new grain structure in a deformed material by the formation and migration of HAGBs driven by the stored energy" introduced by plastic deformation is termed as recrystallization [17]. Recrystallization may occur heterogeneously with clear nucleation and growth stages, and in this case it is described as a discontinuous process. On the contrary, it can also take place uniformly such that the microstructures evolve progressively with no clear nucleation and growth stage, exhibiting a continuous character. Static recrystallization (SRX) refers to the recrystallization process during annealing while that occurred during deformation at elevated temperatures is called dynamic recrystallization (DRX). During the early stages of annealing, fine dislocation-free crystallites are formed by SRV, these nuclei grow and consume the strain hardened matrix, driven by the stored energy associated with the dislocations and/or sub-boundaries. This process is the most studied and widely used recrystallization process, which can be classified as discontinuous static recrystallization (DSRX). SRX can also take place homogeneously without clear nucleation and growth stage, a good example is when Al alloys with particle-stabilized subgrain structure are annealed at elevated temperatures. Fine particles precipitate out along grain/subgrain boundaries, gradual subgrain growth takes place during subsequent annealing due to the coarsening of dispersoids (reduced pinning force) and LAGBs misorientations increase progressively until they are transformed into HAGBs. In this way, a new microstructure develops uniformly throughout the deformed matrix, and is therefore labelled as continuous static recrystallization (CSRX) or extended recovery.

Back to DRX, the definitions of these three types of DRX processes is given in the introduction section, i.e., discontinuous dynamic recrystallization (DDRX), continuous dynamic recrystallization (CDRX) and geometric dynamic recrystallization (GDRX). It will not be reiterated here, but more details will be given for each DRX process in later sections. It is worth noticing that, if the straining is stopped after the critical strain for DDRX but the annealing temperature does not drop sufficiently fast, the recrystallization nuclei produced in the material will grow with no incubation time into the matrix with higher stored energy. This phenomenon is known as metadynamic recrystallization (MDRX) or post-dynamic recrystallization (PDRX) [18], which will not be further discussed in this review due to the space limitation.

It has been realized for many years that the nuclei of recrystallization are not formed by random atomic fluctuations as for the case of phase

Table 1
SFE of common metals and alloys measured at room temperature [35].

Metal	γ_{SFE} (mJ m^{-2})	Metal	γ_{SFE} (mJ m^{-2})
Aluminium	166	Zinc	140
Copper	78	Magnesium	125
Silver	22	91Cu:9Si	5
Gold	45	Zirconium	240
Nickel	128	304 Stainless steel	21
Cobalt (FCC)	15	70Cu:30Zn	20

transformations, but small volumes which already exist in the deformed microstructure [1]. For these small volumes, usually subgrains, to successfully become growing new grains, it is necessary to have a high angle misorientation, as well as an energy advantage. The classical theory of strain induced grain boundary motion (SIBM) proposed by Beck and Sperry [22], which involves the bulging of part of pre-existing HAGB that is associated with a single subgrain possessing large size to provide the energy advantage, further confirmed this. For SRX, this energy advantage can be built through SRV by subgrain growth [23] or subgrain coalescence [24–26]. The time needed to form the large subgrains such that the driving force due to the stored energy is sufficient to overcome the boundary curvature, according to the classic work of Bailey and Hirsch [27], is termed as incubation time to indicate the initiation of recrystallization *during SRX*. This definition is, however, no longer convenient for DRX, thus the critical strain (ε_{cr}) or critical dislocation density (ρ_{cr}) is often used to define the onset of recrystallization, which will be described in more detail in the following sections. After defining the key terminology within the recrystallization domain, the factors influencing DRX are now summarized in the following section.

2.2. Factors influencing DRX

2.2.1. Stacking fault energy

The stacking fault energy (SFE, γ_{SFE}) of the material has a significant effect on DRX. The stacking fault is a textbook knowledge in physical metallurgy, but it may not be equally clear for researchers outside this field. To facilitate the discussion, perfect close-packed planes and their arrangement in an FCC metal are shown in Fig. 1. After the first layer A, there are two types of triangular-shaped voids (represented by the red and black triangles in Fig. 1) that can be occupied by the next layers.

In the FCC structure, the sequence of planes is A, B and C, where plane B and Plane C each take the position of one type of voids, as shown in Fig. 1. A perfect dislocation slips in the {111} planes along ⟨110⟩ directions, e.g., from B1 to B2 ($\vec{b}_1$), as shown in Fig. 1. However, for energetic and topographic reasons, it is favorable to split the dislocation into two so-called partial dislocations or Shockley partial dislocations: displacement of atoms from B1 to C ($\vec{b}_2$), and then from C to B2 ($\vec{b}_3$), as illustrated in Fig. 1. The energy (E) of a dislocation is ~Gb^2. The dissociation of perfect dislocations according to Fig. 1 is:

$$\vec{b}_1 = \vec{b}_2 + \vec{b}_3 \rightarrow \frac{a}{2}\left[\bar{1}10\right] = \frac{a}{6}\left[\bar{1}2\bar{1}\right] + \frac{a}{6}\left[\bar{2}11\right] \tag{1}$$

Obviously, $b_1^2 > b_2^2 + b_3^2$ and, thus the dissociation of the dislocation is favored energetically. However, we also have to account for the additional energy (γ_{SFE}) introduced by the stacking fault, which has a higher energy than the normal lattice, this energy prevents the partials spread too far. The stacking fault width (d) is defined by the balance between repulsive forces acting between the partial dislocations and attractive force due to γ_{SFE} [28]:

$$\gamma_{SFE} = \frac{Ga^2}{24\pi}\frac{1}{d} \tag{2}$$

The γ_{SFE} thus determines the extent to which unit dislocations dissociate into partial dislocations. Typical γ_{SFE} values of various metals and alloys (at room temperature) are presented in Table 1. It should be mentioned that measuring precisely the γ_{SFE} is difficult due to the small separation distance between partial dislocations, alternate methods have been proposed [29–31]. It is even more challenging to measure γ_{SFE} at high temperatures due to the additional change of elastic constants and microchemistry, as well as the pinning of dislocations by solutes or impurities. Little data are available in the literature on this aspect, the reported γ_{SFE} values usually show a very large scatter [32], they

were reported to increase, decrease or even keep constant with increasing temperature, depending on the investigating materials [30,33,34].

During recovery, the stored energy of the material is mainly lowered by annihilation and rearrangement of dislocations into lower energy configuration, both of which are achieved by glide, climb and cross slip of dislocations. For materials with high γ_{SFE}, such as Al alloys, α-iron and nickel, the dissociation of the perfect dislocation into two partials is more difficult and perfect dislocation glide, climb and cross slip takes place readily. During deformation at elevated temperatures, rapid DRV occurs readily which generally prevents the accumulation of sufficient dislocations to sustain DDRX. Well-developed subgrain structures are observed during deformation with only limited dislocations within them, and the misorientation of subgrain boundaries progressively increases which may lead to HAGBs at larger strains, this process is known as CDRX. If the material of high γ_{SFE} is deformed to a large strain with *significant reduction in one direction*, e.g., by hot rolling or hot compression, then the original grains become elongated and GDRX can take place.

On the other hand, low γ_{SFE} will promote the formation of wider stacking faults, which makes the cross-slip or climb more difficult, materials of this type include silver, austenitic stainless steels etc. For these materials, it is difficult to form subgrain structures during deformation by DRV, instead, the dislocation density increases to a high level and eventually some of the local differences in dislocation density become large enough to overcome the capillary term to allow the formation of new grains. Finally, a new microstructure is obtained, this dynamic process is known as DDRX.

In summary, the SFE determines the width of stacking fault which influences the level of dislocations dissociation into partial dislocations. Low γ_{SFE} promotes such a dissociation reaction which hinders the climb and cross slip of dislocations, i.e., retards DRV. This explains why CDRX and GDRX are generally observed for high γ_{SFE} while DDRX is expected for materials with low γ_{SFE}. It should be emphasized that γ_{SFE} is not the only factor to determine which type of DRX processes will take place during hot deformation, other influencing factors, which also play important roles in DRX, will be discussed in the following sections.

2.2.2. Initial grain size

One of the most well-known effects of initial grain size is its strengthening effect on yield stress (σ_y) through the Hall-Petch relation [1]:

$$\sigma_y = \sigma_0 + \frac{k_y}{\sqrt{d}} \tag{3}$$

where σ_0 is a material constant, k_y is the strengthening coefficient, d is the average grain size. Grain boundaries impede dislocation movement, so by varying the grain size it is possible to modify the ease of dislocation motion and yield strength. This obviously applies to all the three type of DRX processes. It has been observed however that the highest yield strength is often obtained when the grain size reaches ~10 nm; the yield strength will either remain constant or decrease with further decreasing grain sizes [36]. In addition to mechanical properties, the initial grain size also affects microstructure evolution of the three DRX processes, but in different ways, as will be discussed below.

During DDRX, grain boundaries are preferred sites for nucleation, so a large initial grain size provides fewer nucleation sites, recrystallization kinetics is slower [37,38]. At the same time, heterogeneities such as deformation and shear bands, which are also sites for nucleation, are more readily formed in materials with large grain sizes [1]. Except recrystallization kinetics, the initial grain size also largely determines the shape of the stress-strain curve during DDRX, i.e., single peak or multi peaks. Sakai and Jonas [39] have reported that if the ratio of the recrystallized and initial grain size (D_S/D_0) is larger than 2 (grain coarsening), an oscillatory stress-strain curve with multi peaks is obtained. Lower ratio of $D_S/D_0 < 2$ (grain refining) leads to a smooth curve with a single peak. It

should be mentioned that the recrystallized grain size (D_S) at steady state is not linked to the initial grain size, instead, it depends sensitively on T and $\dot{\varepsilon}$ which determines the steady state flow stress. This means the same recrystallized grain size will be obtained if the samples of different initial grain sizes are deformed at the same condition, either by grain coarsening or grain refinement. The initial grain size also plays a role in determining which type of DRX processes takes place during hot deformation. For example, decreasing the initial grain size from 35 μm to 8 μm leads to the transformation of DDRX to CDRX for 304 austenitic stainless steel [12].

The effect of initial grain size on CDRX is not as substantially studied as its DDRX counterpart. The effect of initial microstructure on grain refinement in 304 stainless steel deformed at 873 K was systematically investigated by Belyakov et al. [40]. They reported that the samples with finer initial grain size exhibit higher yield stress and approach to steady-state stress more quickly. Smaller grain size was found to accelerate the kinetics of grain refinement, i.e., the increase of misorientation for LAGBs is faster, which was also observed when compressing AZ31 Mg alloy at 573 K [41] and Mg—8Gd—3Y—0.4Zr at 673 K [42]. Simulations show that the steady state grain size is independent of the initial grain size [4,43]. Experimental proofs on hot deformation of different metallic materials confirm that the recrystallized grain size does not depend on the initial grain size when the CDRX proceeds to some degree [40,44].

It is known that when a polycrystalline metal is deformed, the grain boundary area increases with increasing strain since the grains change their shape according to the macroscopic shape change during deformation. For instance, the grains of a rolled specimen become elongated along the rolling direction (RD), the grain thickness (H) in the normal direction (ND) is related to the strain (ε) and the initial grain size (D_0) by the following Eq. (1)

$$H = D_0 \exp(-\varepsilon) \tag{4}$$

Note that the ε used here is the true strain along ND and not the equivalent von Mises strain. The cell or subgrain size formed during deformation changes very little at large strains [45,46], although it depends on the temperature and strain rate, the grain thickness (H) decreases much faster and finally reaches to the size of 1 ~ 2 subgrain size. If the deformation is performed at high temperatures, GDRX will then take place. It can be seen that a small initial grain size (D_0) will reduce faster the boundary space (H) to the critical value for GDRX.

2.2.3. Thermo-mechanical processing conditions

Most of the laboratory studies on DRX are focused on constant TMP conditions, i.e., the deformation temperature and strain rate are kept unchanged during the whole DRX processes. It is convenient to incorporate the strain rate ($\dot{\varepsilon}$) and deformation temperature (T) are into a single parameter - Zener-Hollomon parameter (Z) for studying DRX, as:

$$Z = \dot{\varepsilon} \exp\left(\frac{Q}{RT}\right) \tag{5}$$

where R is the gas constant, Q is an "deformation" activation energy that is often above the self-diffusion of the investigated material, A, α and n are material constants. The flow stress (σ) can also be related to Z through the Sellars and Tegart constitutive equation, i.e., $Z = A(\sinh \alpha \sigma)^n$ [47]. In general, for the DDRX regime, flow stress curves of multiple peaks appear when T is high and $\dot{\varepsilon}$ is low (low Z), and single peak flow stress curves exhibit if low T and high $\dot{\varepsilon}$ (high. A steady state is reached for materials with these two types of flow curves at large strains, and this steady state is dependent on Z. For CDRX and GDRX, the stress-strain curves are much less documented since the large deformation needed is usually performed by severe plastic deformation (SPD) methods such as equal channel angular pressing (ECAP), or high pressure torsion (HPT), which do not allow recording the stress-strain curve. Hot torsion tests can also be used to reach large deformation as long as the temperature gradient is small enough along the gauge length section. According to the limited available data, it is shown that a steady state of stress is attained at large strains during CDRX even when deformation was performed at cryogenic temperatures for Cu [18], no obvious peak being observed. A sharp stress peak was observed just after yielding during multi directional forging (MDF) of AA 7475 at a strain rate of $3 \times 10^{-4} \, s^{-1}$, followed by work softening at temperatures higher than 573 K during CDRX. The steady state flow stress also decreases with deformation temperature, while its variation with strain rate is mostly unexploited [48]. On the other hand, when deforming an Al alloy with 99.7% of Al, 0.18% Fe and 0.07% Si by hot torsion at 400 °C where GDRX is the main recrystallization mechanism, it was found the flow curves show a strain hardening to an approximate steady state regime when the strain reaches near $\varepsilon = 1$ and the stress starts declining from $\varepsilon = 3$ to $\varepsilon = 60$ [49].

The recrystallized grain size at steady state (D_S) of DRX, which is of great importance to the mechanical properties of the material such as strength, ductility etc., is also closely related to the deformation conditions typically expressed as a function of Z. A large amount of empirical
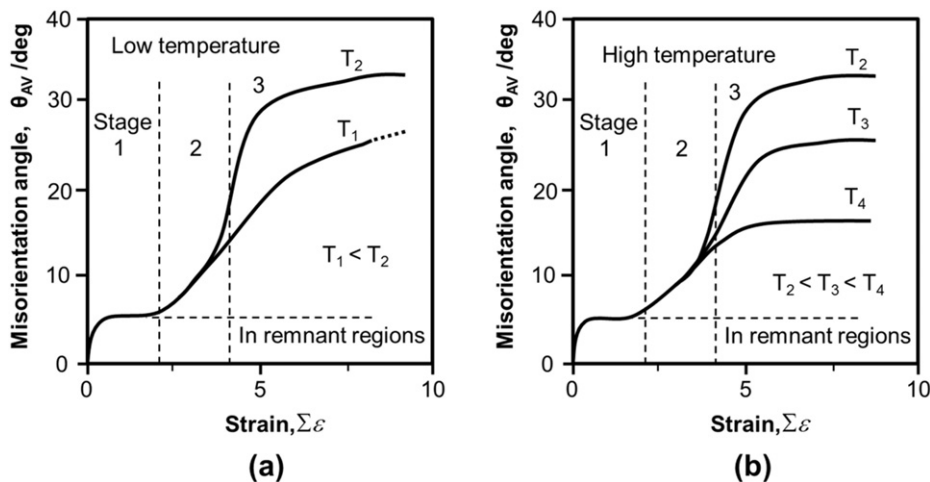
Fig. 2. Schematic graph showing the evolution of deformation induced (sub)boundary misorientation θ_{AV}: (a) at relatively low temperatures in highly alloyed materials containing fine particles, and (b) at high temperatures above $0.5Tm$ in lightly alloyed materials [18]. The values of θ_{AV} in the interiors of the initial grains are indicated by the broken line [55]. (Reprinted with permission from Elsevier [18]).

equations express this relationship in the literature, for different materials. As mentioned above, the steady state stress (σ_S) can also be related to Z in a similar way. A well-known relationship between the normalized steady state flow stress and the normalized grain size for a wide range of materials, is reported by Derby [50,51]:

$$\frac{\sigma_S}{G} \cdot \left(\frac{D_S}{b}\right)^{2/3} = K_2, 1 < K_2 < 10 \qquad (6)$$

where G and b are the shear modulus and the Burgers vector. Deviation from this simple relationship (constant K_2) between grain size and stress was reported when the stress and strain rate in the sample are not homogeneous [52].

As compared to the extensive literature data on stress-strain curves and final recrystallized grain size, the influence of deformation temperature and strain rate (in constant conditions) on recrystallization kinetics and grain size during DDRX is less systematically investigated. The microstructure evolution during DDRX of austenitic stainless steels, in terms of recrystallization kinetics and grain size evolution, was characterized by optical microscopy and EBSD at different deformation conditions in Refs [53,54]. In general, recrystallization kinetics increases with increasing deformation temperature and decreasing strain rate. The recrystallized grain size increases with strain and approaches to the steady state value at ~10% of recrystallization; the steady state grain size increases with increasing deformation temperature and decreasing strain rate. During CDRX, it is the evolution of the LAGB misorientation distribution that matters for the change of microstructure during deformation. It was found that deformation temperature affects the LAGB misorientation in different ways, as schematically illustrated in Fig. 2. The mechanisms behind will be discussed in more details in Section 4 when detailing with CDRX. The effect of strain rate on the evolution of LAGB misorientation is, however, mostly left unexploited.

The deformation temperature and strain rate may determine the DRX mechanism in some materials. This has been observed in different materials such as ZK60 Mg alloys [11], AZ31B alloys [56], commercial pure Mg [57], Inconel 690 [58], 316(N) stainless steel [59] etc. For ZK60 Mg alloys, low temperature (<473 K) DRX is related to the operation of twinning, CDRX was observed in the intermediate temperature range (473–523 K) while DDRX dominates at temperatures above 573 K. Actually, since the DRX mechanism changes with the Z-parameter, the dependence of recrystallized grain size on Z also changes.

DRX at variable conditions has attracted more and more interests since it is closer to industrial practices. For instance, the strain rate is not at all constant during hot rolling, it decreases rapidly when the maximum strain is approached [60]. The effect of changing strain rate on stress-strain behavior was investigated by Urcola and Sellars [61–63] using a ferritic stainless steel, pure Al and Al-1% Mg, they reported that the mechanical equation of state ($Z = A(\sinh\alpha\sigma)^n$) was only followed for the ferritic stainless steel and Al-1% Mg under conditions of changing strain rate, i.e. pure Al did not follow it. In terms of microstructure evolution during and after changing the strain rate, subgrain size and dislocation density inside subgrains are not exclusively related to flow stress, which is the case during hot deformation at constant strain rate. This means numerical models using the average dislocation density (or similar quantity) as the only state variable will not be capable to describe the (sub)microstructure evolution in the case variable deformation conditions. The new equilibrium subgrain size can only be obtained after some transient strain following the strain rate change; this delay becomes more significant when the strain rate is decreased. Systematic work on this topic were conducted later by Sellars and his co-workers [64–67]. Deformation at variable conditions for Armco iron and silicon steel also revealed that both the mean subgrain size and dislocation density within the subgrains evolve [68]. Huang and Humphreys [69] reported that DRX by strain induced grain boundary migration, i.e. DDRX, can take place for specimens of commercial purity Al when subjected to large strain rate reduction during high temperature deformation. Other than changing deformation temperature and strain rate, the effect of changing deformation path on DRX was also investigated and it was found that DRX can be delayed by strain path change [70].

2.2.4. Second-phase particles

It is well known that second-phase particles play a big role in recrystallization. Fine dispersoids tend to hinder boundary motion and slow down recrystallization and grain growth through a Zener drag effect [71,72]. The Zener pressure is proportional to $\gamma_{GB} \cdot V_f / \bar{r}$, where γ_{GB} is the grain-boundary energy, V_f is the particle volume fraction and $\bar{r}$ is the mean size of the particles. By contrast, coarse constituent particles can accelerate recrystallization by particle stimulated nucleation (PSN) due to the large amount of stored energy in the deformation zone [73]. The solute drag effect, on the other hand, reduces the mobility of the boundary in a more complex manner, depending on grain boundary velocity. Both Zener pinning by fine particles and solute drag by alloying elements in solution slow down the grain boundary migration. A comparison of the effectiveness of Nb solute and NbC particles on impeding grain boundary migration in Nb steels was done by Hutchinson et al. [74]. Since there is little direct evidence of the occurrence of PSN during DRX [75–77], the rest of this review will only focus on fine particles and solute effects.

There have been only a few systematic studies on the effects of solutes on DRX. To exclude the contribution from precipitation, the effect of solute can be studied for alloys at temperatures higher than the equilibrium solution temperature. Luton and Sellars [78], Le Gall and Jonas [79] examined, respectively, the effect of 5–20% Fe and 0.2–20 ppm S additions on the DRX of Ni, Gao et al. [80] examined the influence of metal purity (4 N–7 N) on the DRX of Cu, and Desrayaud investigated the influence of carbon content on the DRX of α-Iron containing various amounts of carbon ranging 5–200 ppm. The overall effects of increasing solute content can be qualitatively summarized as follows: i) broadened peak of flow stress; ii) increased peak stress and peak strain, as well as steady state stress; iii) the proportionality constant (K) between the steady-state stress and steady-state grain size (see Eq (6)) depends on solute content.

A large number of studies have been dedicated to the use of second-phase particles to control the microstructure and thus mechanical properties through DRX in Nb microalloyed steels [81], Ni-based alloys [82–84], Mo-bearing steel [85], oxide dispersion strengthened (ODS) steels [86], Al alloys [87] etc. A typical example is the retardation of recrystallization by fine precipitates to increase the temperature of no recrystallization (T_{nr}) during hot rolling of steels [88]. This is because large deformation can then be applied to the austenitic structure, leading to austenite pancaking, and strain induced transformation to form fine ferrite [89]. The presence of precipitates also increases the flow stress of the material [90], as well as the austenite grain coarsening temperature [91]. Another example concerning the effect of fine and coarse second phase particles on grain refinement during ECAP of an Al—Mg—Mn alloy through CDRX, studied by Nikulin et al. [92]. The tests were conducted using strain intervals from 1 to 12 at a temperature of ~573 K. Extensive grain refinement under ECAP was obtained through CDRX when a dispersion of fine Al_6Mn particles was present. In contrast, a coarse recrystallized grain structure was observed in the material with coarse Al_6Mn particles due to the discontinuous growth of recrystallized grains (i.e., PDRX) during the intervals between the ECAP passes.

The particle/matrix interfacial character also affects the DRX behavior. Miura et al. [93] investigated the recrystallization behavior of two Cu alloys, which containing coherent and incoherent precipitates respectively, deformed from 723 to 973 K at true strain rates between 4.1×10^{-4} and 3.2×10^{-2} s^{-1}. DRX took place more easily in Cu containing incoherent precipitates than in the other alloy with coherent particles, due to the stronger interaction between dislocations and the coherent particles. However, the transformation of the coherent

precipitates into incoherent ones can be realized by the spread of recrystallization at larger strains.

The effect of fine second-phase particles on DRX varies depending on whether they exist before the onset of recrystallization, form during the progress of recrystallization, or after the completion of recrystallization. During DRX where concurrent precipitation takes place, the recrystallization driving force and the Zener pinning force are evolving with time. According to the classical Zener pining theory, the size and spacial distribution of the particles are assumed to be uniform which is never the case in reality. Precipitates might dissolve into solution and re-precipitate again later, such as during the weld thermal cycle during friction stir welding (FSW) where CDRX is often an important mechanism for grain refinement [94]. Due to these complexities, numerical models are developed to help understanding the effect of second-phase particles on DRX [85], which will be discussed in more detail in the following sections.

2.3. Characterization of DRX

When analyzing DRX processes, it is routine work to examine, among the others, the flow stress curve, the onset of recrystallization, the recrystallized grain size, recrystallized fraction and/or the evolution of the distribution of LAGB and HAGB misorientations. A systematic description on the characterization of DRX is, however, still missing in the literature. In what follows, the characterization of key quantities used to describe DRX processes is addressed, including some of the recently emerged techniques. The standard preparation procedures for the metallography are not included in this review since it is not unique to DRX.

A lot of information can be obtained by just looking at the flow stress curves during DRX. One should take care of the possible deformation heating generated during tests at fast strain rates. Only relatively small homogeneous deformation can be reached by tensile and compression tests, after which necking or barreling may take place. The torsion test can normally give very large deformation, and the stress-strain curve is usually converted from the torque-twist data through the Fields and Backofen method [95], which is not above criticism neither [96,97]. During DDRX, the peak and critical strains depend on the Z parameter and the ratio of critical strain to peak strain was empirically found as ~0.5–0.8 [1]. Poliak and Jonas developed a very accurate method to detect the onset of DRX using the double-differentiation technique [98], which was in principle based on concepts from thermodynamics of irreversible processes. This approach was subsequently simplified by Najafizadeh and Jonas [99]. The steady state recrystallized grain size can be predicted once the associated flow stress is known, using the Derby relationship discussed in Section 2.2.3. As will be discussed in later sections, a few model parameters, e.g., the parameters in the work hardening model, can be derived from the flow stress curve.

In terms of recrystallized grain size and recrystallized fraction for DRX, they are usually characterized by optical microscopy, SEM with EBSD, or TEM. A detailed work on quantitative metallography of SRX, including the nucleation kinetics, growth rate of recrystallizing grains etc., can be found in Ref [100]. A full description of the characterization of DRX is still missing in the literature. When the recrystallized grains are too small or they become unidentifiable with the old deformed grains, the use of EBSD or TEM is necessary. The advantage of EBSD and TEM techniques is that they can reveal the substructure inside the deformed grains, and thus makes it *possible* to distinguish the recrystallized and non-recrystallized grains using criteria combining grain size, grain shape, misorientation inside the grains, etc. A review on characterizing deformation strain, i.e., deformed or non-recrystallized grains, with different methods using EBSD was given in Ref [101]. It should be noted that, when preparing the thin sample for TEM analysis, care should be taken to avoid deforming the sample. When making comparison with literature data on recrystallized grain sizes, attention should be paid to whether the grain sizes involved are of 2D or 3D nature, they should be converted to the same type if they are not consistent. It

is beneficial to have relatively large initial grain size for studying DRX since it is easier to distinguish the recrystallized grains from the deformed old grains just according to their difference in size. However, it should be noted that, when processed in the same conditions, the onset of DRX takes place later and recrystallization kinetics is slower when the grain size is larger. This might pose a problem if the fully recrystallized state, which requires a large deformation that is usually not matched by conventional mechanical testing method, is of interest since strain localization or fracture of the sample usually occurs prior to that. The recrystallized area fraction can be directly considered as volume fraction according to stereographic principles [102,103]. Another point to consider for characterizing the recrystallized grain size and recrystallized fraction is the quench delay after the termination of deformation, which is particularly important when deformation is performed at high temperature with large strain rate. In these conditions, PDRX takes place without incubation time and can complete within 2 s, which is usually the minimum time needed to quench the sample below the recrystallization temperature. For this reason, the recrystallized fraction or softening fraction is also frequently estimated by indirect methods such as double hit experiment [104–106], or stress relaxation experiment [107].

The evolution of LAGB misorientation is also an important aspect to examine during CDRX. Its characterization usually requires TEM and/or EBSD. The subgrains are typically equiaxed micron-sized volumes bounded by thin dislocation walls, i.e., LAGBs. The variation of the misorientation of these LAGBs has been mostly characterized by diffraction in the TEM before the emergence of EBSD, where only a small number of misorientation measurements were usually made, and they are thus criticized as lacking statistical reliability. Depending on the grain orientation, solute, initial grain size and deformation temperature, deformation and microshear bands [1], which form major nucleation sites for recrystallized grains, might form even during hot deformation. More importantly, a high misorientation usually develops across the deformation and microshear bands, which should be distinguished from the progressive increase of subgrain boundaries misorientation.

In terms of advanced characterization of recrystallization, conventional EBSD with automated focused ion beam (FIB) [108–110] or manual [111] serial sectioning to reveal full 3D microstructures, however most of the studies are focused on SRX [109,111,112]. During DRX, the recrystallized grains are usually small, which makes it more difficult for the 3D reconstruction after serial sectioning. The 3D X-ray diffraction (3D-XRD) method, which is a synchrotron X-ray technique emerged over the past decade, has been used to resolve the nucleation and growth of individual recrystallization nuclei during SRX, as illustrated for deformed AA 1050 [113]. In-situ observation of DRX at has been conducted using a confocal scanning violet laser microscope [114], transmission polarized light microscopy [115], X-ray diffraction patterns [116], Electron Channeling Contrast Imaging (ECCI) [117], and by recording the microstructure evolution in video format [118]. The in-situ EBSD studies on microstructure evolution during both hot deformation and annealing were reviewed by Wright and Nowell [119]. In terms of hot deformation, most of the studies are focused on small strains [120], the increasing surface roughness of the sample makes it difficult to index the microstructure using EBSD at large strains. The effect of the free surface on recrystallization behavior is also of concern during these in-situ studies. However, from a number of preliminary *in situ* hot-tensile experiments on Al alloys, it has been shown that the *in situ* experiments on Al alloys are consistent with what is observed using bulk materials [121].

3. Discontinuous dynamic recrystallization

3.1. Introduction

When it is not specifically pointed out, DRX refers in general to the conventional DDRX process which has clear nucleation and growth
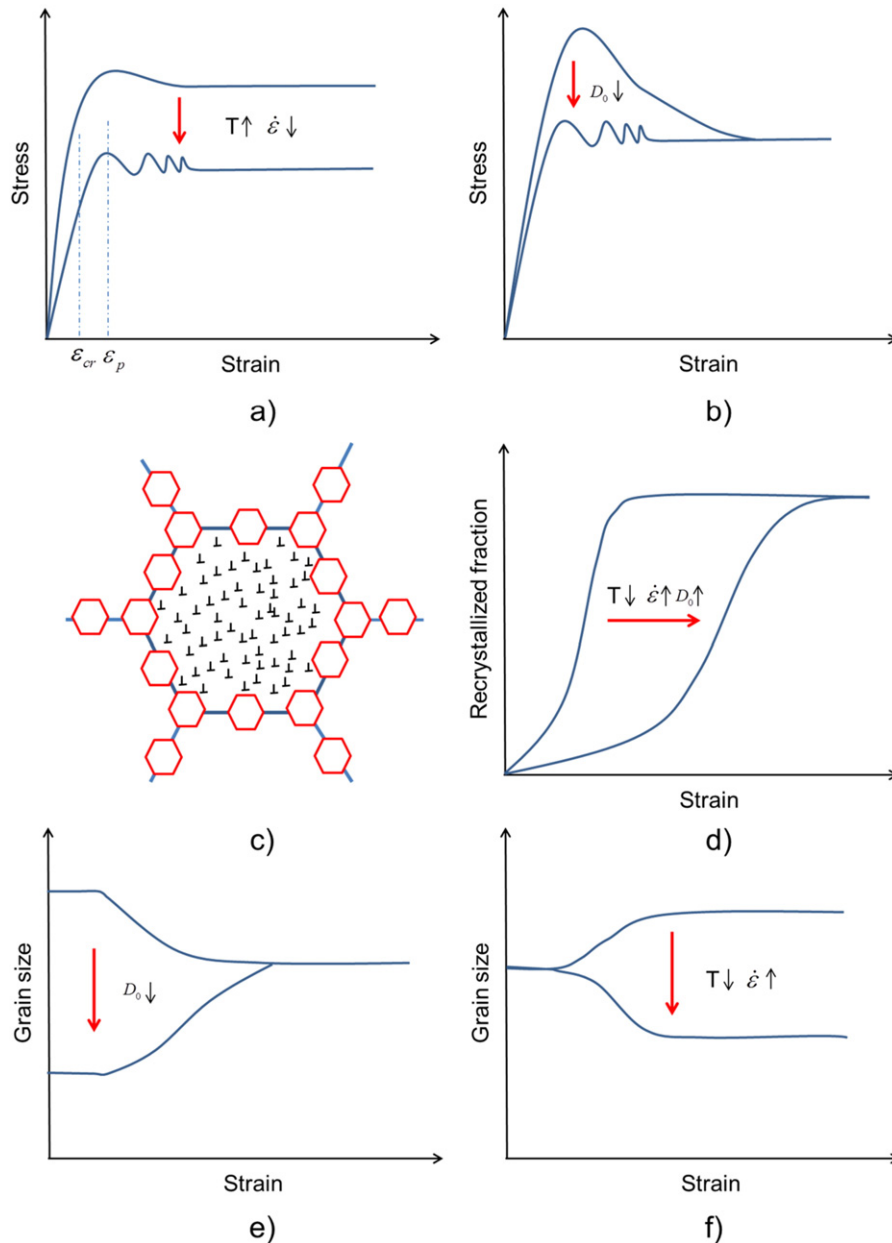
Fig. 3. Schematic illustration of the typically observed experimental characteristics of DDRX with changes in deformation conditions ($T,\dot{\varepsilon}$) and initial grain size (D_0): a) and b) stress–strain response showing the transition from single to multiple peaks; c) The necklace structure during DDRX; d) Effect of deformation conditions and initial grain size on recrystallization kinetics; e) evolution of average grain size depending on the initial grain size D_0; f) evolution of average grain size depending on deformation conditions. Note that a steady-state size D_s is reached in e) and f).

stages. DDRX usually occurs during hot deformation of low to medium SFE alloys. Alloys that undergo DDRX exhibit a number of general characteristics which are well-established by experiment; they are schematically illustrated in Fig. 3 and can be summarized as follows:

i) A critical strain ε_{cr}, somewhat lower than the peak strain ε_p, must be reached before DDRX occurs [122,123]. Both this critical strain and peak strain decrease steadily with decreasing Zener-Hollomon parameter [124].

ii) Depending on the deformation temperature, applied strain rate and initial grain size of the material, single peak or multiple peaks may be observed in the stress–strain response. The steady state stress is correlated to the Zener-Hollomon parameter, and it is independent of the initial grain size [125]. (Fig. 3a and b)

iii) Nucleation of DDRX is usually initiated at pre-existing grain boundaries, a necklace structure [126] of equiaxed grains forms when there is a large difference between the initial grain size and the recrystallized grain size (Fig. 3c).

iv) Recrystallization kinetics accelerates with decreasing initial grain size [125,127] and strain rate, as well as increasing deformation temperature [124] (Fig. 3d).

v) During DDRX, the grain size evolves toward a saturation value D_s which then does not change as recrystallization proceeds. Either grain refinement or grain coarsening takes place depending on the initial grain size and deformation conditions [128]. A power-law relationship between the steady-state grain size and Zener-Hollomon parameter (or stress) is usually observed [12,125,129], even though deviation at high Z values was also observed [124] (Fig. 3e and f).

3.2. Mechanisms

3.2.1. Work hardening and DRV

In this section, we start with a brief overview on work hardening and DRV, the details of which are out of the range of this review, interested readers are referred to Refs [46,1]. The occurrence of DDRX depends on the accumulation of dislocations in the deforming materials. Two competing processes take place simultaneously: the continuous generation of dislocations during deformation, i.e. work hardening, and DRV in the form of dislocation annihilation:

$$\frac{d\rho}{d\varepsilon} = \frac{d\rho^+}{d\varepsilon} + \frac{d\rho^-}{d\varepsilon} \qquad (6)$$

The critical dislocation density can be reached for materials with low γ_{SFE} since DRV is less rapid, as detailed in Section 2.2.1. This leads to the onset of DDRX [131–134], where nuclei will form on grain boundaries or other internal crystal defects such as shear bands, deformation zone around large particles, i.e., the sites associated with large stored energy.

The variation of the dislocation content and structure is the most significant change occurring during DRX. The dislocation density is often related to the flow stress according to:

$$\sigma = \sigma_0 + \alpha\mu Mb\sqrt{\rho} \qquad (7)$$

where σ_0 is a frictional stress, α a constant depends on the geometrical arrangement of the dislocations, μ the elastic shear modulus, M the Taylor factor and b the Burgers vector. The dislocation density, ρ, is usually considered as a single parameter for materials with low γ_{SFE} [3,135], meaning that ρ can reasonably be considered as homogeneously distributed. This is not the case for high γ_{SFE} materials, as will be discussed in Section 4. The dislocation density of typical metallic materials in fully annealed state is ~10^{11} m^{-2}, which increases to as high as ~10^{16} m^{-2} if the materials are heavily deformed [1]. Such changes are of great importance in industrial practice, and for the understanding of the subsequent DDRX processes. The evolution of ρ is widely described by the Kocks-Mecking (KM) model, which reads in its original form as:

$$\frac{d\rho}{d\varepsilon} = \frac{d\rho^+}{d\varepsilon} + \frac{d\rho^-}{d\varepsilon} = k_1\sqrt{\rho} - k_2\rho \qquad (8)$$

The storage term, $k_1\sqrt{\rho}$, is related with the athermal storage of moving dislocations. The basis of dislocation storage is that during
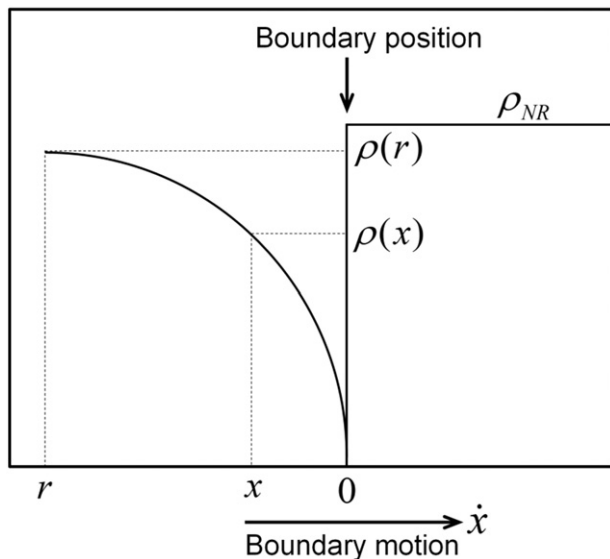

Fig. 4. Schematic diagram of the dislocation density variation at a dynamic recrystallization front (Reproduced with permission from Elsevier [133]).

deformation a given mobile dislocation travels a distance proportional to the average spacing between the dislocations $1/\sqrt{\rho}$. This is mean free path of dislocations (L). The first term on the right side in Eq. (8) is equivalent to $d\rho^+/d\varepsilon = 1/bL$, or $d\rho^+/dt = \dot{\varepsilon}/bL$. The annihilation term, $k_2\rho$, is associated with DRV, a process that is thermally activated so it is not surprising that k_2 is dependent on temperature and strain rate. A more complicated theory, considering the energy barrier for dislocation annihilation, has also been presented to predict the dislocation annihilation rate in pure metals [136]. Three conventionally used equations for predicting the dislocation density evolution, including the KM equation, describing strain hardening and DRV, were compared by Montheillet et al. [137]. It is worth noticing that, even during hot deformation, static recovery of the Bailey-Orowan type, in which the annihilation of dislocations is proportional to the deformation time, was also included as a third term in Eq. (8): $r/\dot{\varepsilon}$ [138], which is equivalent to $d\rho/dt = -r$, where r is the static recovery coefficient. The assumption that DRV is prevalent for most of the applications is, however, employed in most of the cases, i.e., the static recovery term is usually neglected.

At constant temperature and strain rate, the work hardening and DRV of metallic materials with low SFE can in general be described using the equations listed above. In variable TMP conditions, which are frequently observed in industrial practice, using only one dislocation density as state variable is not able to accurately predict the microstructure evolution [46,130,139], this will be detailed in Section 3.3.3.

3.2.2. Grain boundary migration

The basic process during the migration of HAGBs can be considered as a transfer of atoms adjacent to the boundary, from the shrinking grain to the growing grain [140]. It is generally accepted that a grain boundary moves with a velocity (v) in linear relation with the effective pressure (P_{Eff}) applied on the boundary:

$$v = mP_{Eff} \qquad (9)$$

with $m = m_0 \exp(-\frac{Q}{RT})$, the boundary mobility, where m_0 is a pre-exponential factor, Q the apparent activation energy, R the gas constant. The effective pressure P_{Eff} is the sum of the driving pressure (P_D) and a retarding pressure (P_R).

$$P_D = E_D = (\rho_2 - \rho_1)\tau \qquad (10)$$

where τ is the energy per unit length of dislocation line. Even though relationships between driving force and grain boundary migration other than (9) were proposed, recent work [141–143] has confirmed that relationship (9) holds for the average grain boundary migration. The grain boundary mobility was shown to be strongly dependent on crystallography, i.e. misorientation of the adjacent grains and orientation (inclination) of the GB in a crystal [143–144]. More details on the mechanisms of grain boundary migration can be found in Refs [145,146]. The effect of second-phase particles and/or solute atoms on grain boundary migration will be discussed in Section 3.3.2.

3.2.3. Nucleation of DDRX

If DRV is not rapid enough to annihilate the dislocations created during work hardening, the dislocation density will keep increasing until a critical DDRX condition, at which the first group of nuclei forms. The critical strain (ε_{cr}^{DDRX}) is usually used to identify this critical condition, instead of the critical dislocation density (ρ_{cr}^{DDRX}). The reason is that ε_{cr}^{DDRX} can be empirically related to the peak strain (ε_p^{DDRX}), which is easy to capture from the flow stress curve; typically one finds a relationship of the type: $\varepsilon_{cr}^{DDRX} = A\varepsilon_p^{DDRX}$, where A is a material constant, this value was found to be ~5/6 [147], but later experiments show that it varies between 0.2 and 0.8 depending on the investigated material. The lower limit of the value was found in polycrystalline copper where the DDRX grains are formed at the triple junctions or non-equilibrium grain boundary junctions [148,149]. The nucleation on serrated grain

boundaries usually starts at a higher strain with A around 0.6–0.8 [129, 150]. Several other attempts have been made to predict the initiation of DDRX through the flow stress analysis, among them the one proposed by Poliak and Jonas [98] and its simplified version [99] are most widely used. It is important to note that the ε_{cr}^{DDRX} identified by this method is not the strain at which the first nuclei appear, but the strain at which a small fraction of recrystallization (1–5%) takes place, this fraction is needed to have a detectable effect on the flow stress [151]. This approach is however still of empirical nature. Below we now examine the nucleation process in a more analytical way.

It is generally accepted that nucleation during DDRX can be initiated through SIBM, which is first reported by Beck & Sperry [22] and subsequently studied by Bailey and Hirsch [27]. This type of theory was first developed based on the observations during SRX, where no further deformation is applied to the areas behind the moving HAGBs. During DDRX, the areas swept by the HAGBs undergo continuous deformation and dislocations keep accumulating in these areas. Sandstrom and Lagneborg [132] proposed a semi-quantitative approach by assuming that DDRX is only possible when the grain boundary migration rate of the potential nucleus is high in relation to the rate of building of dislocations behind it. Following their model, Roberts and Ahlblom [133] further analyzed the critical condition for DDRX without second-phase particles. As shown in Fig. 4, the high angle boundary is migrating from left to right into unrecrystallized material with a high dislocation density of (ρ_{NR}) with velocity of $\dot{x}$. The dislocation density of the potential nucleus behind the moving boundary drops to a minimum value, however, concurrent deformation of the material raises the dislocation density behind the moving boundary following some function $\rho(x)$, tending towards a critical dislocation density value of ρ_{cr}^{DDRX}.

To begin with a simple case, a spherical nucleus of radius r is considered. The driving force for the grain boundary migration is related to the dislocation density difference, i.e., stored energy difference across the boundary. Since the dislocation density is uneven behind the moving boundary, the radial average of the dislocation density is considered, and the difference in stored energy is:

$$\Delta E = \frac{\tau}{r} \int_0^r (\rho_{NR} - \rho(x)) dx \tag{11}$$

where τ is the dislocation line energy. The net free energy change related to nucleation is:

$$\Delta G(r) = -\frac{4}{3}\pi r^3 \cdot \frac{\tau}{r} \int_0^r (\rho_{NR} - \rho(x)) dx + 4\pi r^2 \gamma_{GB} \tag{12}$$

where γ_{GB} is the grain boundary energy per unit area. The variation of dislocation density behind the moving boundary was first estimated by neglecting DRV, and according to Section 3.2.1, the dislocation storage can then be estimated as:

$$\frac{d\rho}{dt} = \frac{d\rho^+}{dt} = \frac{\dot{\varepsilon}}{bL} \tag{13}$$

As discussed earlier, the grain boundary migration can be expressed by combining Eqs. (9) and (10):

$$\frac{dx}{dt} = v = mP_{Eff} = m\tau(\rho_{NR} - \rho(x = 0)) \approx m\tau\rho_{NR} \tag{14}$$

Dividing Eqs. (13) by (14) gives

$$\frac{d\rho}{dx} = \frac{\dot{\varepsilon}}{bLm\tau\rho_{NR}} \tag{15}$$

And then

$$\rho(x) = \frac{\dot{\varepsilon}}{bLm\tau\rho_{NR}} \cdot x \tag{16}$$

Substitution of Eqs. (16) into (12), and differentiation to find maxima in $\Delta G(r)$ leads to:

$$-r_c\tau\rho_{NR} + \frac{2}{3}r_c^2 \frac{\dot{\varepsilon}}{bLm\rho_{NR}} + 2\gamma_{GB} = 0 \tag{17}$$

which gives a real critical size r_c only if

$$\rho_{NR} \geq \left(\frac{16\dot{\varepsilon}\gamma_{GB}}{3bLm\tau^2}\right)^{1/3} = \rho_{cr}^{DDRX} \tag{18}$$

This critical dislocation density is not likely to be real since a sphere nucleus was considered during the development of Eq. (18). There is good evidence that DDRX is initiated by bulging of pre-existing grain boundaries. By replacing the sphere in Eq. (12) with a bulging nucleus, we find instead

$$\rho_{cr}^{DDRX} = \left(\frac{20\dot{\varepsilon}\gamma_{GB}}{3bLm\tau^2}\right)^{1/3} \tag{19}$$

If DRV is considered according to Eq. (8), no analytical solution can be found for the critical dislocation density, and this value must be approximated through an iterative method, this was treated in Refs [152, 153]. Still considering grain boundary bulging as the only mechanism for nucleation of DDRX, Cram et al. [3] proposed that nucleation of DDRX takes place once the subgrain located on a grain boundary reaches a critical radius. This will be further discussed in Section 3.3.

DDRX was also observed to occur through grain boundary bulging/sliding [154,155], in a way similar to the mechanism involved in CDRX in an earlier observation [156]. During plastic deformation, fluctuations in boundary shape are produced because of the incompatibilities between grains. The developed fluctuations prevent further grain
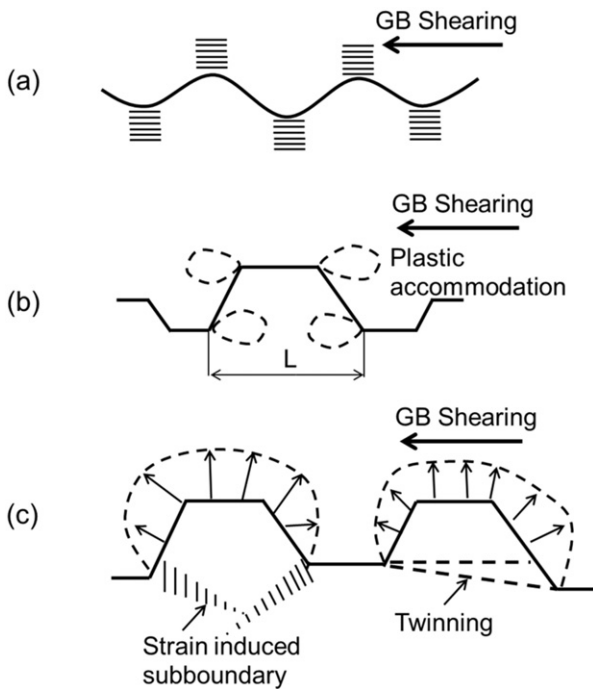

Fig. 5. Schematic graph showing the nucleation of DDRX grain [154]. (a) Boundary corrugation accompanied by the evolution of sub-boundaries. (b) Partial grain boundary sliding/shearing, leading to the development of inhomogeneous local strains. (c) Bulging of parts of a serrated grain boundary accompanied with the evolution of dislocation sub-boundaries or twinning, leading to the formation of a new DDRX grain (Reproduced with permission from Elsevier [155]).
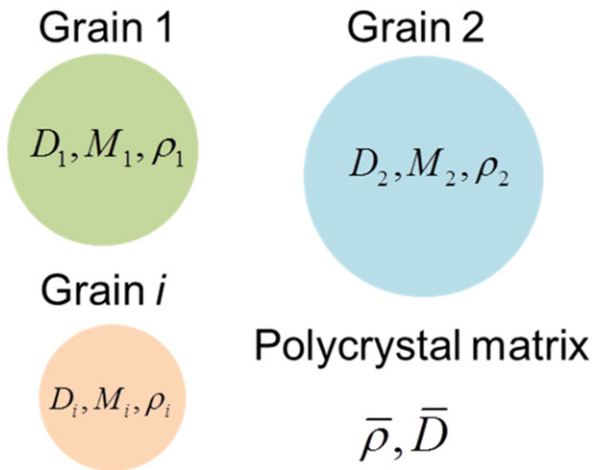
Fig. 6. Schematic illustration of grains immersed within an average polycrystal matrix aggregate (average medium). *Di* is the grain size, *Mi* is the orientation/Taylor factor and *ρi* is the dislocation density (Reproduced with permission from Elsevier [3]).

Fig. 8. The subgrain size distribution within each grain of average radius $\bar{r}$. The hatched area represents the fraction of subgrains larger than the critical size *rc* (Reproduced with permission from Elsevier [3]).

boundary sliding or shearing, dislocations then accumulate leading to high dislocation density gradients followed by subgrain formation near the original grain boundaries, as illustrated in Fig. 5a. Local concentration of strains is developed owing to the continuous deformation, and partial grain boundary sliding or shearing takes place, resulting in additional inhomogeneous strain (Fig. 5b). Under low temperature or high strain rate deformation, strain induced subgrain boundary can then be formed. In contrast, twinning is favoured under high temperature or low strain rate deformation. As shown in Fig. 5c, the DDRX nucleus will form by the bulging of a part of the serrated grain boundaries assisted by the additional inhomogeneous strain. To the best knowledge of the authors, DDRX by grain boundary sliding has not been quantitatively expressed at this moment.

Except for these two generally accepted theories, other new nucleation mechanisms were only occasionally discussed in the literature. These mechanisms usually can only be applied to certain conditions and thus suffer from lack of generality. For instance, a so called heteroepitaxial dynamic recrystallization (HERX) was found in the commercial γ- γ' nickel based super alloy deformed under sub-solvus conditions, with the combination of Energy Dispersive Spectrometry (EDS) and EBSD mapping technique [157]. A coherent γ shell is first formed prior to deformation on the primary precipitates γ' (due to phase transformation), which subsequently behaves as recrystallization nucleus during hot deformation. The nucleus then grows coherently with the parent γ' precipitate.
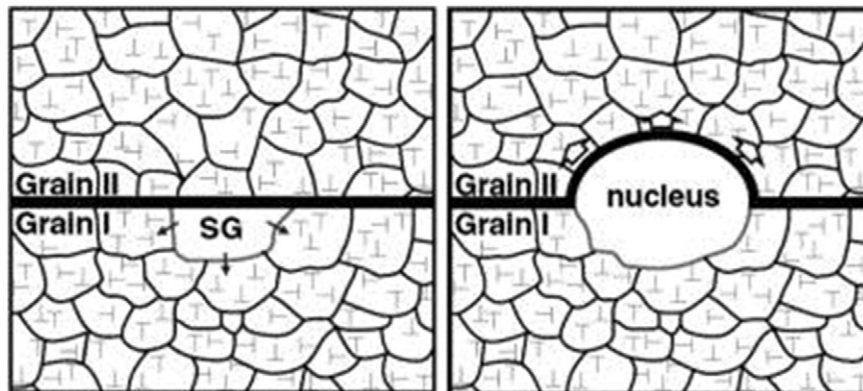
It follows that most of the investigations are focused on the mechanism by which the first recrystallized grains were formed at pre-existing grain boundaries. The nucleation mechanisms explaining the progress of DDRX after the prior grain boundaries were entirely occupied with new grains are mostly left unexploited, only a limited published work exists in the literature on these aspects [158–162]. Brunger et al. [159] observed fractions of 20% of twins at the interface between initial grains and dynamically recrystallized grains using TEM observation when austenitic steel alloy 800H was compressed to a strain of 0.49 at 1100 °C with strain rate of 0.1 s^{-1}. This indicates the importance of twinning for the nucleation of DDRX. The twin frequencies at the front of the recrystallized regions and in the center of such regions were quantitatively compared by Wang et al. [160], it was observed that the twin frequency was higher at the recrystallization front where the twins are most recently created and thus less affected by deformation. This confirms that twinning is an active nucleation mechanism during DDRX process, and the increase in DDRX volume fraction occurring through the formation of multiple twinning chains drives the continuous progress of the recrystallization front. This is illustrated by the case of austenitic Ni-30% Fe model alloy investigated within the DDRX regime using hot torsion testing, by Hodgson et al. [161]. They confirmed that in the necklace mechanism, the subsequent DDRX layers

Fig. 7. Schematic illustration of a subgrain growing (left) and once it reaches the critical size (right) bulging into the deformed matrix as a new strain-free grain [173] (Reprinted with permission from Elsevier [3]).
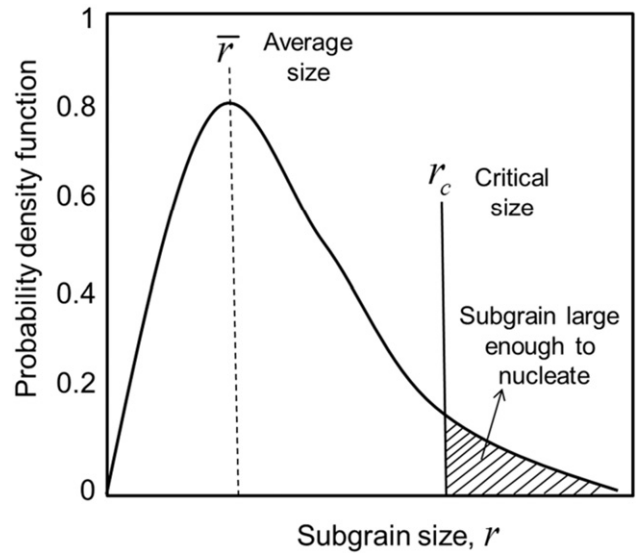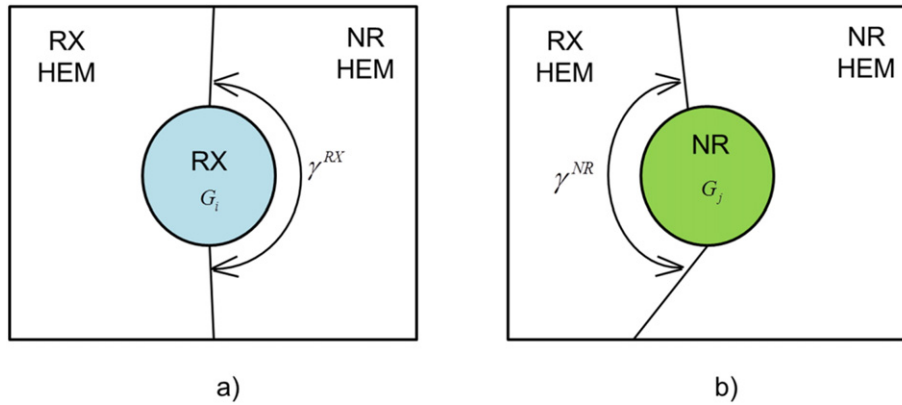
Fig. 9. Illustration of mobile surface fractions (a) as related to a recrystallized representative grain (γ^{RX}), and (b) as related to a non-recrystallized representative grain (γ^{NR}) (Reprinted with permission from Elsevier [153]).

after the first one appear through the repeated nucleation and growth of annealing twins on the migrating interface.

3.3. Numerical models

3.3.1. Constitutive, analytical and empirical models

There are a vast number of DDRX models existing in the literature, a large part of them belong to the constitutive, (semi-)analytical and empirical models [163–166]. In these models, physically based nucleation law and grain boundary migration driven by stored energy difference are usually not considered, instead, the Avrami formalism (JMAK approach [167–170]) or modified Avrami approach [171] is used to describe the kinetics of DDRX. The yield stress, steady state stress, as well as the critical stress for the initiation of DDRX is usually dependent on the Zener-Hollomon parameter Z through empirical equations. Only the final recrystallized grain size can be predicted since it is also dependent on the Z parameter, i.e., it is not possible to know the grain size evolution.

Modeling of a processing step may need several constitutive functions depending on the complexity of the flow curves. Moreover, for multistep processes, altered constitutive constants may be needed for different passes, due to inter-pass softening. This points out the need to incorporate microstructure concepts into the constitutive models. In the following sections, focus will be given to physically based models where the three minimum ingredients to build a DDRX model are all incorporated: work hardening and recovery (stored energy), nucleation law, grain boundary migration law.

3.3.2. Physically based DDRX models without considering second-phase particles

The research in DDRX is mainly driven by the requirements of metal forming industry where quantitative and physically based models are needed to design, control and improve the microstructure and mechanical properties of the final products. From the large number of existing models [3,152,153,172], focus is given to those with physically based nucleation law and proved prediction capabilities in terms of strain-stress curve, recrystallized fraction and grain size, which together characterize the DDRX process.

The DDRX process has been modeled and validated with experimental data in literature by Cram et al. [3]. In their model, the polycrystal metal is represented by a set of spherical grains embedded in a *single* homogeneous matrix whose properties are obtained by averaging all the grains in the aggregate, as illustrated in Fig. 6. Each grain is defined by its size, Taylor factor, dislocation density and subgrain size distribution.

A novel aspect of in this model is the proposed nucleation law during DDRX. Grain boundary bulging was considered as the only mechanism. It was assumed that nucleation takes place when a subgrain located on a grain boundary reaches a critical radius, r_c, which corresponds to the moment when the stored energy difference between the growing subgrain in grain I and deformed matrix in grain II is large enough to overcome the capillary force of the subgrain, as shown in Fig. 7.

The subgrain size distribution in each grain was approximated by a Rayleigh distribution [174], as illustrated in Fig. 8. The subgrains with a size greater than the critical size will have the potential to nucleate, but only those lying on the grain boundary can eventually grow as nuclei. The average subgrain size within each grain evolves with deformation, with a tendency to increase due to subgrain growth and an opposite tendency to decrease due to the increase of stress. Meanwhile, the stored energy driving nucleation also changes during deformation. This means the number of subgrains that can grow as real nuclei in each grain also changes with deformation.

The prediction power of the model was tested against literature data on DDRX in pure Cu with different initial grain sizes, deformation temperatures and strain rates. The key features that characterize DDRX, such as single to multiple peak stress transitions with increasing deformation temperature and decreasing strain rate, unique steady-state stress and grain size with different initial grain sizes, and power-law relationship between stress and grain size, are reproduced in a quantitative way by the model [3]. This model was further developed by the same authors by considering the effects of solute atoms [175], as will be discussed later on.

A two-site mean model of DDRX was proposed by Logé et al. [152, 153,176]. The model considers all key elementary physical phenomena at the grain scale involved during hot deformation, including work hardening and recovery, nucleation and grain boundary migration, as detailed in Section 3.2. A set of representative grains, defined by their size and dislocation density, is used to represent the real microstructure. The surrounding of the representative grains is idealized using two homogeneous equivalent media (HEM) with different dislocation densities, as schematically shown in Fig. 9. Topological information is partially incorporated into the model by considering the relative weight of these two HEM as a function of their volume fractions. A physically based, non-constant nucleation law was used. Nucleation takes place at grain boundaries once the critical dislocation density, which takes DRV into account and thus differs from Eq. (19), is reached for any deformed grain. During nucleation, the number of created recrystallized grains depends on the size and dislocation density of the deformed grain. This approach differs from other mean field models using only one equivalent medium [3,172] where the heterogeneous microstructural effects such as necklacing are not captured. The model is applied

to the prediction of DDRX in 304 L austenitic stainless steel. Good agreement with experimental data has been obtained at different temperatures and strain rates, in terms of recrystallization kinetics, recrystallized grain size and stress–strain curve.

3.3.3. DDRX models considering the effects from solutes and second-phase particles

Besides the above mean field models, a novel method based on thermostatistical approach was developed to describe hot deformation of FCC alloys undergoing DDRX [177]. Nucleation of recrystallization is activated once a critical incubation strain for recrystallization is applied. The dislocation density evolves with strain using a function taking into account the deformation temperature, strain rate and composition. In this model, multicomponent effects are incorporated into the equation to account for solid solution strengthening, as well as their effect on recrystallization. The model is tested against experimental data in terms of stress–strain curves of six different alloys, at intermediate and high temperatures. The proposed theory successfully describes the dynamic recrystallization behaviour of these alloys in terms of stress-strain curves. The effect of the initial grain size on recrystallization kinetics is not included in the model, since it only describes the coarse-grain or single crystal case. The evolution of the recrystallized grain size and recrystallization fraction was considered separately in later works [178,179]. The effect of solute drag on recrystallization during hot deformation of Nb microalloyed steels has been studied and simulated using a microstructure model by Bäcke [180]. The investigations were focused at temperatures where precipitation of Nb(C, N) do not occur. In this model, subgrains are formed during deformation, and their sizes decreases with increasing deformation. DRV is retarded by solute atoms, and the driving force for grain boundary migration is reduced by both the Zener pinning and solute drag. Nucleation of recrystallization is triggered once the subgrains reach a critical size. The numerical results were compared to experiments, and it was shown that the calculated flow stresses for compression tests showed good agreement. However, the evolution of grain size was not presented, even though it can be predicted by the model. In terms of microstructure evolution, a series of Cu—Sn alloys has been used to investigate the effect of solute on DDRX by Cram et al. [175]. In this study, hot compression tests were conducted and the microstructure was characterized using optical and scanning electron microscopy. The qualitative effects of the solute additions on DDRX agree with the reported general observations [78–80]. The physically based model for DDRX of pure Cu [3], detailed in Section 3.3.1, has been extended to include the effect of Sn solute atoms. The effect of solute on the plastic response of the material and the mobility of HAGBs was incorporated. It was concluded that Sn also retards the nucleation of DDRX, and this was realized in the model by considering that Sn atoms may segregate to the dislocations in the subgrain boundary, while their binding with the vacancies that mediate the subgrain motion retards the kinetics. With all these effects, the model predicts well the stress-strain curves and the microstructural evolution at most of the processing conditions, except at lower temperatures with higher strain rates where the model overestimated the stress. Further work is needed to clarify this lack of discrepancy.

The effect of precipitation on recrystallization is more frequently investigated and simulated for SRX, e.g., [181–185]. As for DDRX, a 3-D cellular automation model of DDRX, considering Zener pinning from fine dispersoids ($\ll 1\,\mu m$) in copper, was developed by [186]. In the proposed model, the microstructure is only resolved at grain scale which means subgrains and particles are not explicitly modeled. The particles are introduced into the model in a statistical sense and the effect of particles was limited to retardation of grain boundary velocity. Since diffusion is much faster along dislocation lines, it will take place first at HAGBs and then LAGBs. The lack of particle-(sub)grain interaction [187,188] makes this model less versatile for application to other particle-containing alloy systems. Nucleation of recrystallized grains is described by a constant rate of nucleation, i.e., it is assumed to be unaffected by particles in the model. It is well known that recrystallization is retarded by fine particles, as discussed earlier in Section 2.2.4. Actually these fine particles may also determine the orientations of nuclei, a fact that is widely studied in SRX of Al alloys [189,190]. Another model for precipitation interactions with DDRX is presented by L'ecuyer and L'espérance [85]. It is based on existing DRX models, but modifications have been performed to consider the pinning effect of precipitates. This leads to an increase of the critical dislocation density for the onset of DDRX, and also a decrease of the HAGBs velocity when compared to precipitate-free systems. Simulations have been carried out and compared with experimental results obtained on an Mo-bearing steel compressed at 875 °C. Qualitative agreement is found. Again, only the potential delaying effect of precipitates on HAGBs migration was considered using the Zener pinning theory. The evolution of precipitate size was neglected, only the evolution of volume fraction of the precipitates was considered. Dislocations play an important role on the precipitation kinetics and both pipe diffusion and nucleation on dislocations are considered. Even though the inhomogeneous dislocation substructure was considered when calculating the precipitation volume fraction, i.e., high dislocation density in subgrains walls and considerably less dislocations in the subgrain interior, the fact that precipitation takes place on subgrain boundaries was not considered when calculating the Zener pinning retarding force.

3.3.4. DDRX models in variable/multi-stage conditions

Most metallic products undergo hot working like rolling, forging and extrusion etc. during some part of their processing history. Industrial hot working practices rarely take place at constant strain rate and temperature. For instance, during hot rolling, the rolls have lower temperature than the billet and thus chill the surface of the billet. Meanwhile, the strain rate varies with the strain from entry to exit of the roll [191]. However, when the strain rate is changing continuously or instantaneously, clear deviation from the mechanical equation of state has been reported [61] even when recrystallization is absent. In addition, hot deformation passes are usually separated by intermediate heat treatments, leading to the so called multi-stage hot deformation where DDRX, SDX and PDRX can all take place. DDRX under changing deformation conditions including changes of strain rate, strain path and the effect of intermediate annealing was experimentally studied [70]. Numerical models of DDRX applied in variable conditions are summarized below.

Let us start with the case where DDRX takes place in variable TMP conditions. As mentioned in the previous sections, most of the DDRX models were developed and validated in constant conditions, they are not sufficiently general to model the transient loading conditions in which the strain rate or temperature is not constant. Although this topic has been studied experimentally in terms of stress-strain behavior and microstructure evolution, most of the models are focused only on the former aspect. In a rare case, a preliminary multiscale hot-working model was developed by Takaki et al. [192]. Both macroscopic mechanical behaviors and microstructural evolution were captured by coupling the finite element (FE) method and the phase-field (PF) method, first in constant conditions. Transient deformation simulation, where strain rate and temperature rapidly change during deformation, was then conducted using the multi-phase-field-dynamic recrystallization (MPF-DRX) model. Qualitative agreement with experimental observation has been reached in terms of the evolution of the stress-strain curve, and the average grain size. DDRX models applied to other complex variable conditions such as non-uniform deformation, two-phase material, strain path change [193,194] etc. is out of the scope of this review.

The second topic, i.e., recrystallization in multi pass conditions, is examined below. The different recrystallization regimes, i.e., DDRX, SDX and PDRX, are all important in multi-stage and should be considered carefully in industrial practice. There are only a few models that can track microstructure evolution in such conditions [151,195]. Roucoules et al. [151] developed a mathematical model to describe the
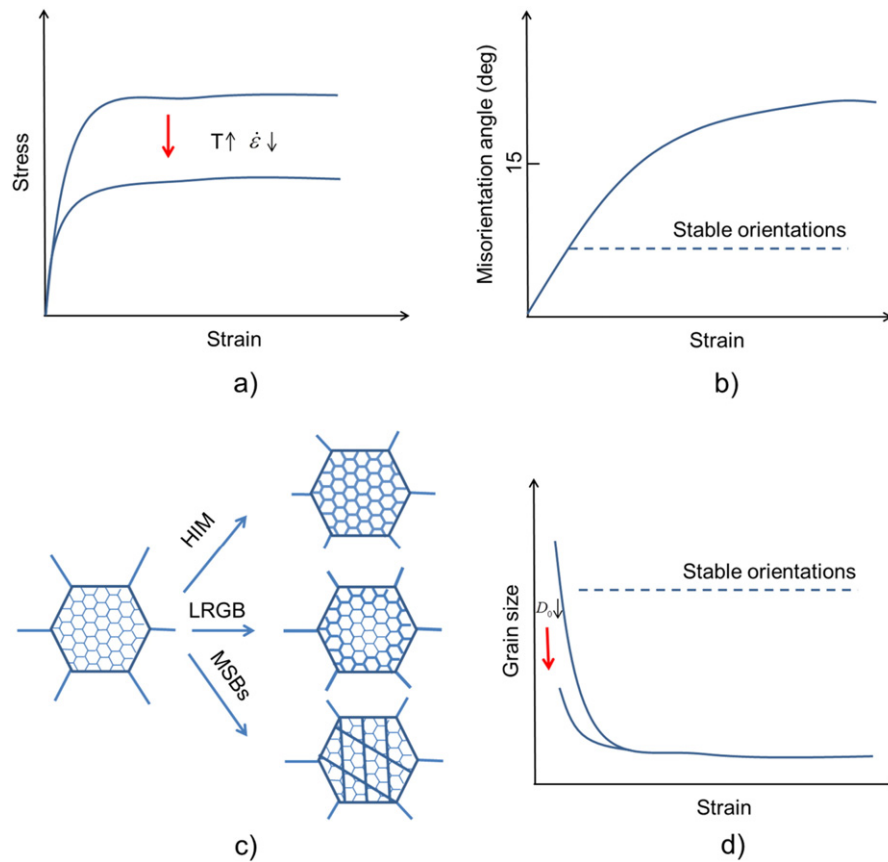
Fig. 10. Schematic illustration of the typically observed experimental characteristics for CDRX: a) stress–strain curve; b) evolution of average strain induced (sub)grain boundary misorientation at high temperatures (>0.5T$_m$); d) forming mechanisms of CDRX, where thin lines represent LAGBs, thick lines represent HAGB or microshear bands; d) evolution of average grain size.

recrystallization behavior during and after hot deformation of austenite where dislocation density was employed as the single internal variable. The model successfully predicted the post deformation recrystallization behavior by varying the process variables such as strain, strain rate and temperature. Unfortunately, experimental data were not explicitly incorporated in the tuning data set. Recently, a novel model which includes as internal state variables both dislocation density and spacing between geometrically necessary subgrain boundaries, was developed by Brown and Bammann [196]. The model predicts both SRX and the DRX. However, little or no attention has been paid to the grain size evolution during different recrystallization regimes for these models [151, 197]. Based on a physically-based two-site mean field DDRX model [152], microstructural evolution due to recrystallization *during* and *after* deformation was modeled by Beltran et al. [152]. The model is able to predict all the key features of recrystallization process including the recrystallized fraction, recrystallized grain size, and flow stress of 304 L austenitic stainless steel during DDRX and PDRX. The model was validated by experimental data, and good quantitative agreement between model predictions and experimental results has been reached. Another model that allows the simulation of multi-stage deformation and predicts recrystallized fraction, grain size and flow stress was developed using the Cellular Automata approach [197].

3.3.5. Summary

This is by no means a comprehensive review on all DDRX models existing in the literature, rather it highlights only the models that can be implemented into finite element softwares to consider the microstructure evolution in any real industrial process, i.e., analytical and empirical models, and physically based statistical models at the grain structure scale. The current status of various approaches to modelling the

recrystallization was summarized by Hallberg [198], where discrete methods such as cellular automata [135,197,199] and Monte Carlo models [200,201], phase field [202,203] and level set [204,205] models of recrystallization, that are not covered in this review, were examined. In recent years, full field models e.g. [206] which cover the crystal plasticity and microstructure evolution are also developed for DDRX. The interpretation of simulation length and time scales in cellular automata and Monte Carlo models is still of challenge, while it is often computationally expensive for phase field, full field and level set models.

It is the current authors' view that an ideal DDRX model should be able to predict, with affordable computational resource, the flow stress curve, evolutions of grain size, recrystallized fraction and crystallographic texture. While many of the existing DDRX models are able to deliver the former three quantities in constant deformation conditions, suitable models that can be used to predict the texture evolution during DDRX are rare. Some attempts have been made to deal with texture issues during DDRX [207–209], however, the evolutions of the other three key quantities used to characterize DDRX are essentially not addressed. Texture control in industrial practice is of great importance for most of the materials due to the significant effect of texture on properties. It is, however, generally accepted that DDRX has the effect of randomizing the texture.

Besides the texture aspect, the importance of twinning for the nucleation of DDRX at large strains approaching to the steady state, which has been observed experimentally for different materials [126,155,210], has not been addressed so far in the existing models. When second-phase particles are involved, their spatial distribution and evolution in size and number density with deformation should be considered. Of equal importance is their retarding effect on grain boundary migration and nucleation of recrystallization, bear in mind that there is little evidence
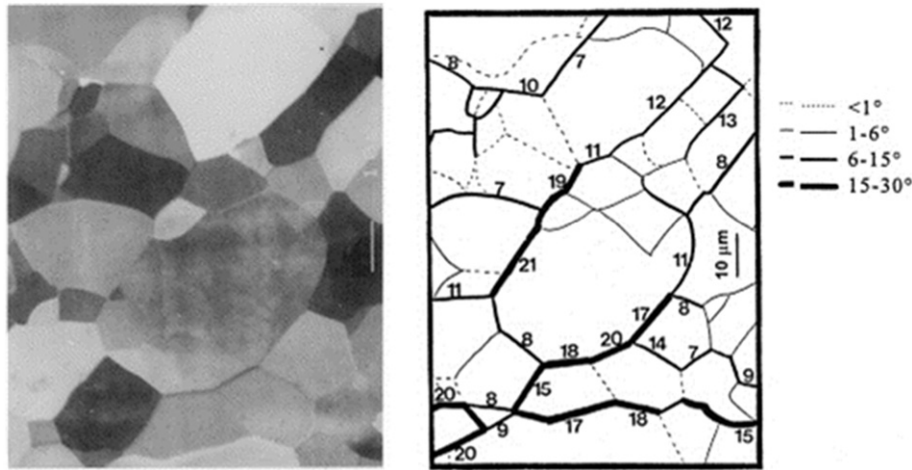
Fig. 11. SEM micrographs and associated misorientation maps of the monocrystalline specimens deformed to $\varepsilon = 1.5$. The single crystal of pure 1199 aluminium has a $\langle 001 \rangle$ parallel to the compression axis which is the vertical direction in this figure (Reproduced with permission from Elsevier [213]).

of PSN during DRX, as discussed already in Section 2.2.4. To take all these aspects into account while still keeping the DDRX model simple is quite challenging during variable deformation conditions, but this appears to be mandatory for industrial metal forming processes applications at high temperature.

4. Continuous dynamic recrystallization

4.1. Introduction

In recent years, it has become evident that new grains with HAGBs may be formed *during deformation* by the progressive rotation of subgrains according to Perdrix [211] and Montheillet et al. [212,213]. In such cases, the microstructure evolves relatively homogeneously throughout the entire material, without recognisable nucleation and growth of the recrystallized grains, and this phenomenon thus falls into the phenomenological classification of CDRX [1]. CDRX is much less investigated as compared to DDRX, since it has long been claimed that DRV is the only softening mechanism in high SFE metals. The time consuming TEM diffraction measurements needed to characterize

the misorientation before the emergence of EBSD technology is another obvious reason [4]. Besides, the large deformation needed to complete or even initiate CDRX usually cannot be matched by general laboratory compression, or tensile tests. SPD is more often needed. Actually, most of the studies on CDRX in the literature are related to SPD techniques like ECAP, HPT, MDF and ARB, for more details on this the reader is referred to the excellent review work by Sakai et al. [18].

The main characteristics of CDRX observed from *hot deformation* can be summarized by considering the following four different aspects [1,4, 11,18,48,156,214,215]:

i) Stress-strain curve: stress increases with strain, and at large strains a steady state stress is reached which increases with decreasing deformation temperature [11,143,214] and increasing strain rate [143,216], and is independent of the initial grain size [40], see Fig. 10a. Single peak was observed on the stress-strain curve for Al and Mg alloys [11,48,217] while no clear peak exhibits for stainless steel [40] and Copper [218].

ii) Average strain induced (sub)grain boundary misorientation: the average misorientation increase with strain [48,219,220], and
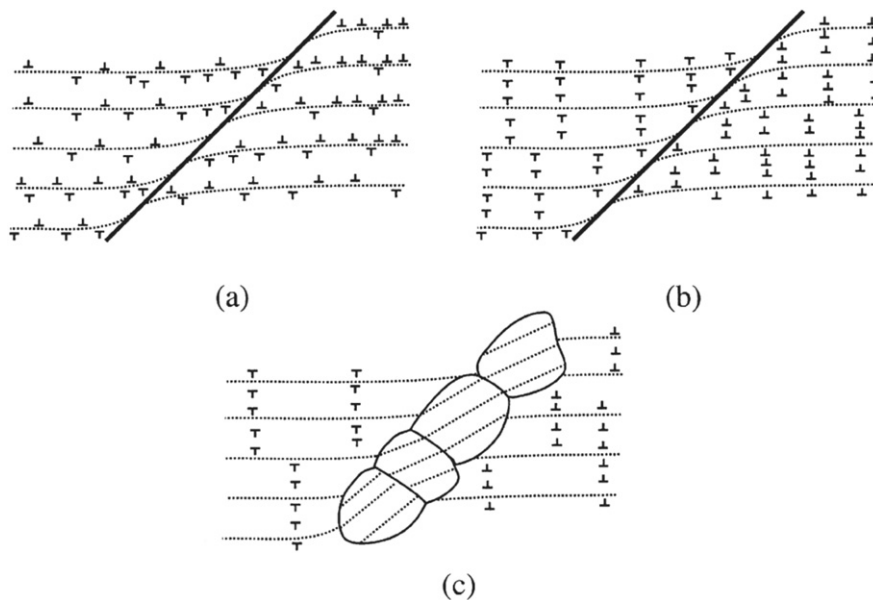

Fig. 12. Schematic diagram showing the proposed mechanism of DRX in magnesium, by progressive lattice rotation and DRV at grain boundaries [52]. (Reprinted with permission from Elsevier [1]).
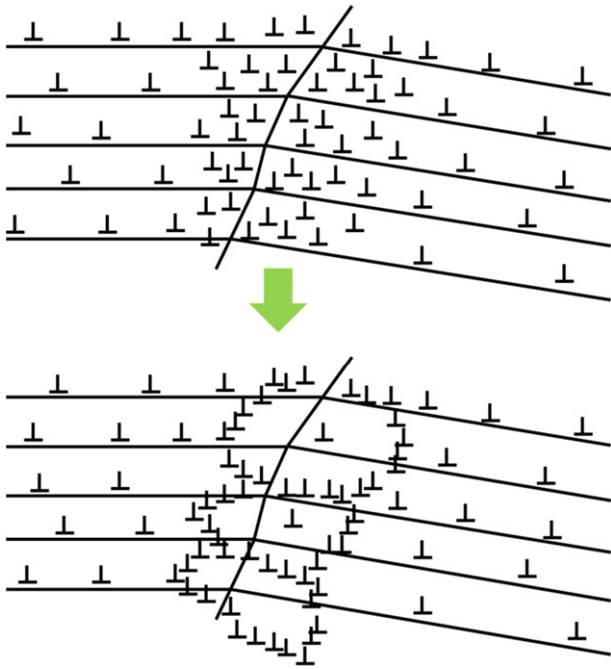
Fig. 13. Schematic diagram showing the CDRX at intermediate temperature for Mg alloy. For simplicity purpose, only dislocations of one sign are shown here. (Reproduced with permission from Elsevier [11]).

low strain rates accelerate this process (when measured as a function of strain) [221], while higher temperatures can either increase or decrease the steady state value depending on the deformation temperature and amounts of alloying elements, as shown in Fig. 2. There exist some stable orientations, for which the increase in misorientation is not sufficient to transform into HAGBs [213,214], as shown in Fig. 10b.

iii) The transformation of LAGBs into HAGBs is reported by homogeneous increase of misorientation (HIM) of LAGBs at very high temperature, by progressive lattice rotation near grain boundaries (LRGB), or by the formation of microshear bands (MSBs) at larger strains, as schematically illustrated in Fig. 10c. It is also reported, in the early stages of deformation, that grain subdivision during hot deformation are strongly affected by the grain orientation [222].

iv) Crystallite size: the average crystallite size decreases with deformation and reaches a "steady value" at large strains (see Fig. 10d), while some stable original grains remain even at large strains [213,214,217]. A decrease in the initial grain size can

accelerate the kinetics of grain refinement significantly under a large strain deformation [40], and the strain path has little effect on the CDRX kinetics [213].

v) Crystallographic texture: a strong crystallographic texture forms at large strains [213,215].

It should be noted that even though there is still some debate on whether CDRX really exists [16], CDRX is actually generally accepted in the community [1,4,11,18,40,94,219,220,223,224]. In what follows, the different mechanisms for CDRX presented in the literature are summarized, together with the attempts to model this process. GDRX, which has many similarities with CDRX and is sometimes classified as one type of CDRX process [1], will be discussed separately in Section 5.

4.2. Mechanisms

4.2.1. CDRX by homogeneous misorientation increase

At relatively *high deformation temperatures*, a homogeneous microstructure usually develops, deformation or microshear bands become less significant as compared to cold deformation. Under these conditions, CDRX occurs by the progressive accumulation of dislocations into LAGBs which increase their misorientation, and eventually HAGBs are formed when the misorientation angles reach a critical value θ_c ($\theta_c \approx 15°$). This mechanism has been observed in Al and Al alloys [213,219], 304-type austenitic stainless steel at 1073–1273 K [6], and microduplex stainless steel [220]. It is difficult to track the evolution of individual LAGB misorientation, the distribution of misorientations of all boundaries after different strains is usually used instead. However, in this case the HAGBs observed after deformation did not necessarily result from progressive increase of misorientation of LAGBs, but could also be due to the evolution of the initial grain boundaries. It is known that the grain boundary area per unit volume increases with deformation [1]. A simple way to disregard the latter possibility is to use single crystal samples, an example of which is shown in Fig. 11, where single crystal of pure Al1199 was hot compressed at 380 °C to a true strain of 1.5. It is clear that a large number of boundaries have a misorientation >15°. A model based on this mechanism was developed by Gourdet and Montheillet [4] and will be detailed in Section 4.3.1.

There is also evidence that the transformation of LAGBs into HAGBs is enhanced when the boundaries are pinned by small particles, which is used to produce fine grain structures that promote superplasticity [1]. This method involves a two-step process, i.e., prior cold and/or warm deformation to increase dislocation density, followed by hot deformation during which subgrains form quickly. The (sub)boundaries are pinned by small particles after a certain deformation level, and dislocations are continuously trapped into these boundaries, which eventually leads to their transformation into HAGBs [225].
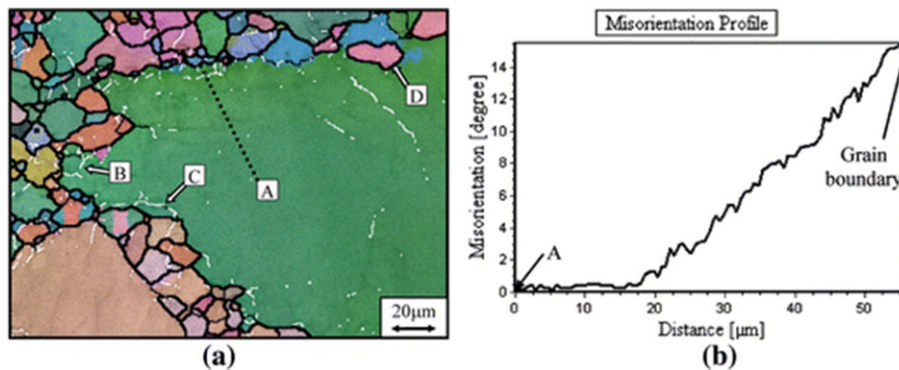

Fig. 14. EBSD measurements revealing evidence of CDRX in AZ31. (*a*) Orientation map of the sample hot compressed to a strain of 0.6 at a temperature of 350 °C and a strain rate of 0.01 s^{-1} (thin white line >2°, thin black line >5°, and thick black line >15°) and (*b*) the cumulative misorientation along the dotted line from A to the grain boundary (Reprinted with permission from Springer [8]).
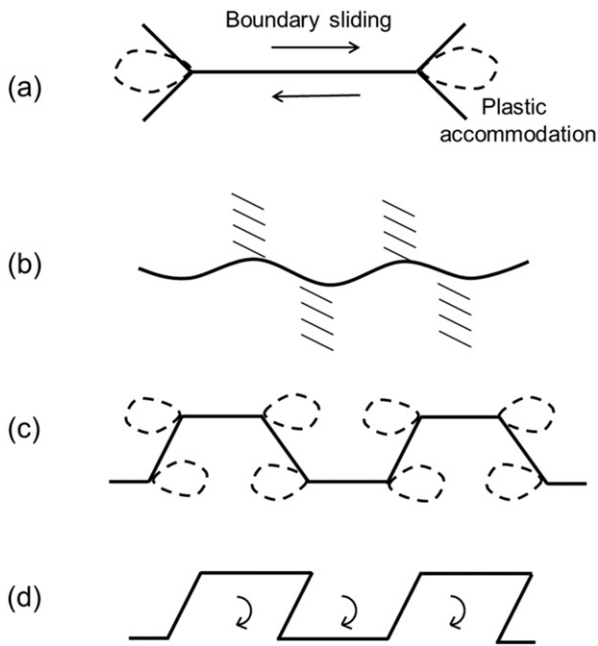
Fig. 15. Schematic graph showing CDRX by local lattice rotation. (a) Grain boundary sliding, leading to the stress concentrations at the triple points; (b) Boundary bulges formed by local migration; (c) Part sliding, and part dislocation motion, leading to mantle formation; (d) Shear of bulges in mantle, leading to asymmetric bulges and local lattice rotation (Reproduced with permission from Elsevier [156]).

4.2.2. CDRX by progressive lattice rotation near grain boundaries

There is evidence that CDRX can be achieved by the progressive rotation of subgrains adjacent to pre-existing grain boundaries during deformation in certain materials, similar to the so called rotation recrystallization that occurs in many minerals [226]. It was reported that in magnesium alloys [52], the progressive lattice rotation occurring at grain boundaries may lead to the formation of new grains. Ion et al. [52] proposed a simple mechanism to explain the formation of new grains during hot deformation of Mg alloys, as illustrated in Fig. 12. Deformation in Mgs alloy is non-homogeneous due to the lack of independent slip systems often found in HCP structures, therefore local shearing first develops near grain boundaries (Fig. 12a). As local shearing proceeds lattice rotation near the boundary, and DRV (Fig. 12b) also takes place to form well defined subgrains in the boundary region (Fig. 12c). Eventually, small amounts of sub boundary migration lead to the coalescence of boundaries and the formation of new grains with HAGBs.

The occurrence of CDRX for Mg alloys deformed in the intermediate temperature range (473–523 K) was later confirmed by [11]. Instead of simply ascribing the formation of subgrains near original grain boundaries to DRV, they went on by stating that the controlling mechanism of plastic deformation and CDRX is cross-slip of dislocations with $\vec{a}$ Burgers vector on non-basal planes, as schematically shown in Fig. 13. The cross-slip process is more activated near original grain boundary regions due to the concentrated stress. During cross-slip, $\vec{a}$ screw dislocation can be transformed to an edge dislocation through the Friedel-Escaig mechanism [227,228]. This edge dislocation can then climb, since it lies in a non-basal plane with high SFE [229,230]. The LAGB network is developed near the original grain boundary region with the help of dislocation rearrangements by cross-slip and climb. The formation of new grains is due to the continuous absorption of dislocations in the LAGBs. It was also pointed out that at high deformation temperatures, more slip systems may be activated and deformation then becomes more homogeneous, which brings back conventional DRX (i.e. DDRX) as the operating mechanism [11].

Microstructural features consistent with these CDRX mechanisms were experimentally observed. As shown in the EBSD orientation map (see Fig. 14a), a large pre-existing grain was decorated by a necklace of dynamically recrystallized grains in AZ31 deformed at 350 °C to a strain of 0.6. A plot of the cumulative misorientation from the interior of the grain (point A) to the grain boundary (along the dotted line) clearly indicates a large increase in misorientation (Fig. 14b). The development of LAGBs close to the necklace near the grain boundary can also be seen, examples are indicated by B and C. These LAGBs may progressively increase their misorientation and transform into HAGBs upon further deformation. Similar misorientation profiles near the grain boundary was also observed for Mg—8Gd—3Y—0.4Zr compressed to a strain of 0.9 at 400 °C and 0.005 s^{-1} [42].

Lattice rotation at grain boundaries during deformation is not exclusive to Mg alloys, it was also reported for instance in Al alloys containing considerable solute additions such as Al—Mg alloys [214,231] and Al—Zn alloys [231]. The microstructure evolution during hot deformation of Al—Mg was explained in the following way [156]. Grain boundary sliding preferentially takes place at favorably oriented boundaries, as schematically shown in Fig. 15a. The migration of HAGBs, driven by the stored energy difference across these boundaries, leads to the formation of serrations (Fig. 15b). Since grain boundary sliding as shown in Fig. 15a can remove the small serrations developed, large serrations or bulges will first be developed on non-sliding boundaries at large strains, as shown in Fig. 15c. Once the bulges are formed, grain boundary sliding can still activate on the protruded parts, and the remaining parts of the boundary have to accommodate the strain by plastic deformation, which leads to local lattice rotation and asymmetric shape of the boundary, and finally to subgrain formation, as shown in Fig. 15d. New grains are formed once the subgrain misorientation becomes sufficiently large. It is interesting to notice that a similar mechanism has also
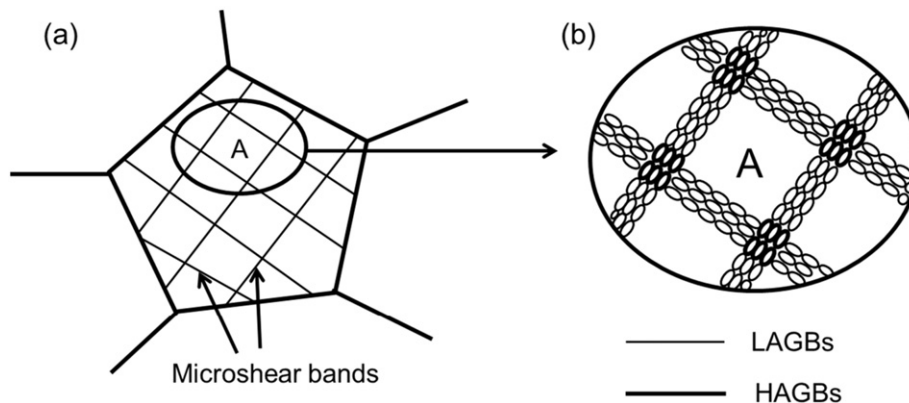

Fig. 16. Schematic drawing of the development of (a) microshear bands at low strains and (b) the subsequent formation of new grains at their intersections and along the bands at sufficiently large strains (Reproduced with permission from Springer [233]).
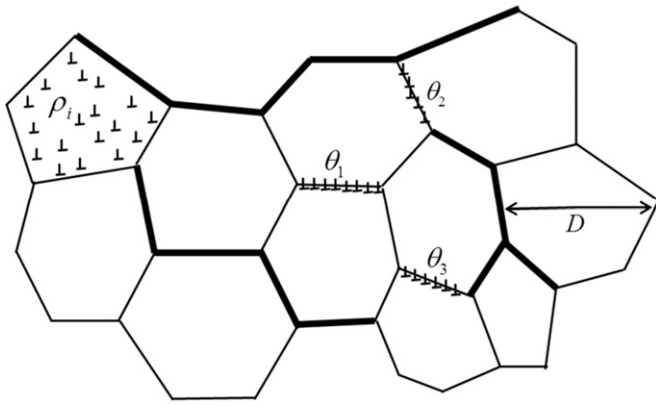
Fig. 17. Schematic representation of the CDRX microstructure illustrating the internal variables of the model: the mean intercept length D, the dislocation density inside the subgrains ρi, and the misorientation angles of the LAGBs. (thick lines: HAGBs, fine lines: LAGBs). (Reprinted with permission from Elsevier [4]).

been used to explain the DDRX process, as shown earlier in Fig. 5. During hot deformation of Al alloys with prior cold and/or hot deformation, the operation of grain boundary sliding along the original HAGBs during early stages of hot deformation, followed by the increase of progressive subgrain rotation was reported by Sakai et al. [216,232].

4.2.3. Microshear band assisted CDRX

Another mechanism of CDRX has also become apparent during SPD to form ultra-fine grained (UFG) microstructures, i.e., microshear band assisted CDRX. The formation of microshear band during hot deformation has been confirmed by optical microscopy, EBSD and TEM [52,233]. The dislocations introduced at low strains are arranged into cellular substructure, which can be considered as an incubation period for the formation of new grains, i.e., stage 1 in Fig. 2. Multiple microshear bands can be formed in the grain interiors leading to the rapid increase in average misorientation, a spatial network of microshear bands result, as shown in Fig. 16a, corresponding to stage 2 in Fig. 2. The subsequent deformation leads to a rapid increase in the density of microshear bands, as well as in the HAGBs and LAGBs. But these phenomena do not take place homogeneously within the material, they mainly appear inside the microshear bands, more so at the intersections of the microshear bands. The fraction of UFG structure increases as deformation proceeds, leading to the progressive propagation of an equiaxed microstructure through the entire volume. One may argue that the formation of microshear bands may be solely due to the change in strain path in SPD processes, e.g., ECAP or MDF, it should be noted that the same phenomenon was observed during rolling of austenitic stainless steel at 873 K [6] and during hot compression of a Mg alloy [52]. It is true, though, that more intersecting microshear bands are formed during SPD processes because of the strain path changes.

Similar to the mechanism described in Section 4.2.2, new grains are actually first formed in heterogeneously deformed zones, i.e., near
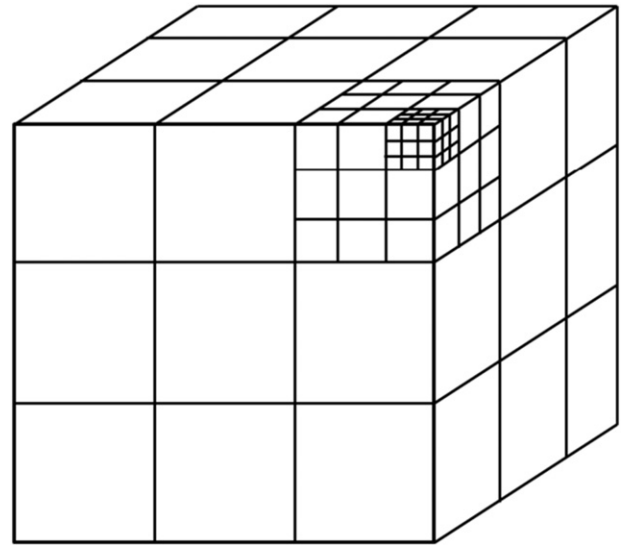

Fig. 19. Subdivision of a cube-shaped grain into 27 subgrains. Next-level subdivision at two smaller scales is also shown for a corner-cube (Reproduced with permission from Elsevier [215]).

original HAGBs or microshear bands. During further straining, they do spread more homogeneously through most of the remaining volume, thereby differing from conventional DDRX where clear two-steps process via nucleation and growth stages of recrystallized grains is involved.

4.3. Numerical models

As compared to the conventional DDRX which has been modelled in different conditions, only a few numerical models are dedicated to CDRX process [4,43,208,234,235]. Two of the CDRX models, which account for the main phenomena such as strain hardening, DRV and HAGB migration (or grain subdivision) and predict key quantities that characterize the CDRX process (including stress-strain curves, grain size and misorientation distribution), are summarized below.

4.3.1. The Gourdet and Montheillet model

A simple CDRX model using the average dislocation density inside the crystallites, the average crystallite size and the distribution of LAGB misorientations as internal variables, focusing on the hot deformation of high SFE metals, is proposed by Gourdet and Montheillet [4]. The material microstructure is represented by a set of so called "crystallites" surrounded partly by low-angle (LABs) and partly by high-angle (HABs) boundaries, as schematically shown in Fig. 17. The dislocation densities inside the crystallites, as well as the crystallite sizes are assumed to be homogeneous, which then evolves during deformation. The evolution of dislocation density inside a crystallite through strain hardening and DRV is described by the Laasraoui-Jonas
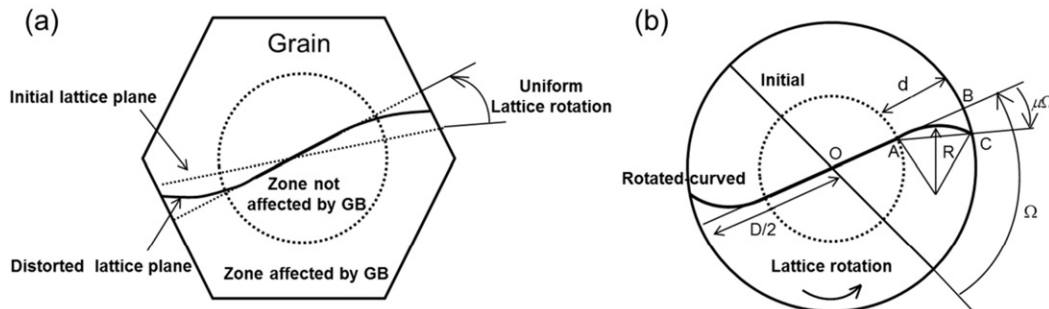

Fig. 18. a) Lattice curvature in a grain; b) Simplification for calculating the lattice curvature (Reproduced with permission from Elsevier [215]).

equation [236], a modification has been made to take HAGB migration into account, which also decreases the average dislocation density by replacing the swept deformed area with a dislocation free zone. A part of the recovered dislocation density contributes to formation of new LAGBs, and the other part is absorbed by the pre-existing boundaries, some of which are annihilated by HAGBs while those incorporated into LAGBs lead to the gradual misorientation increase of LAGBs into HAGBs. The predictions of the model are presented for both the transient and steady states, including stress-strain curves at various constant temperatures and strain rates, as well as the associated evolutions of microstructural quantities such as crystallite size, dislocation density and LAGB misorientation distribution. The effect of HAGB migration on these parameters is emphasized.

This model links the stress-strain curve to key microstructural parameters and is capable to predict the evolution of crystallite size, dislocation density and misorientation distribution with strain, under different constant hot deformation conditions. However, crystallographic texture effects were neglected, and the fact that LAGB is able to migrate, as demonstrated when the stress or strain rate changes during deformation [69], was neglected in this model. The idea that LAGBs keep increasing the misorientation during hot deformation until they are transformed into HAGBs was challenged by McQueen and Kassner [16], since no experimental validation of the model was provided. McQueen and Kassner [16] claim that GDRX is a better mechanism to explain the observed microstructure evolution. The increase of LAGB misorientations is mainly related to transition boundaries (microshear bands), which increase their misorientation rapidly and become similar to original HAGBs. However, later experimental work conducted by Kaibyshev et al. [219] on Al—Li—Mg—Sc alloy using Equal-channel angular extrusion at 300 °C to a total strain of 12 confirmed the progressive evolution of LAGBs into HAGBs. Similar observation was reported in a 304-type austenitic stainless steel subjected to rolling at 1073–1273 K [6].

4.3.2. The Toth et al. model

A different model of CDRX based on grain fragmentation has been developed by Toth et al. [215], predicting the evolution of the grain size distribution, misorientation distribution, crystallographic texture and strain-hardening of the material. The basic assumption is that lattice rotation within an individual grain is not uniform during deformation because of the constraining effects of the neighbouring grains and grain boundaries. The lattice rotation is different near the grain boundaries than in the grain interior, this difference increases progressively with strain. A crystallographic plane is curved near the boundary zone and becomes a near S-shape surface, which gives rise to lattice curvature, as shown in Fig. 18a. Different boundaries may impede the rotation of a lattice plane in a non-uniform way, different curvatures of the lattice plane thus result. For simplification purpose, a spherical grain shape is assumed with diameter D and with grain boundary affected zone of thickness d, as shown in Fig. 18b. The lattice curvatures $(1/R)$ within a grain are accommodated by the so called curvature-induced dislocations. The increase of these dislocations eventually leads to the appearance of strain-induced boundaries. If the middle zone and grain boundary zones are of equal size, i.e., $d = D/3$, the subdivision of a grain in 3D can be simplified as a "Rubik cube" as shown in Fig. 19, where only the central element has no grain boundaries. On this basis, a fragmentation scheme is developed which is integrated into the Taylor viscoplastic polycrystalline model.

This model gives good predictions in terms of grain size and grain misorientation distribution during ECAP at *room temperature* for technical purity copper. The crystallographic textures after deformation are also well reproduced, and the flow stress of the material is also reliably predicted, through the modelling of dislocation density evolution coupled with texture development. Dislocation density evolution is followed for each grain using a multi-phase dislocation cell approach, i.e., dislocation density in the cell interior (ρ_c), the cell-wall dislocation

density which is further split into statistical dislocations (ρ_{ws}) and the geometrically necessary dislocations that build misorientations between neighbouring cells (ρ_{wg}) but not the mesoscopic lattice curvatures, and finally the non-mobile curvature-induced dislocations.

In their model, once the misorientation between adjacent elements reaches 5°, the element is considered to become an independent grain which can lead to further grain refinement. This is because all the elements belong to one grain are assumed to have the same slip distribution and strain-hardening characteristics, obviously this assumption does not hold true at large values of strain. This critical value of 5° is relatively low, care should be taken when performing quantitative comparison with experimental results. Also, the model is not likely to be applicable to very large deformations, since the Taylor model of a polycrystal, which usually fails at very large strains, was used [215]. It is thus not clear whether it can predict the occurrence of a CDRX steady state and describe the latter properly.

4.3.3. Summary

A careful examination of these two CDRX models, i.e., Gourdet and Montheillet (GM) model [4] and Toth et al. model [215], reveal a few key differences. First, new grains are distributed relatively homogeneously in the former model, while they develop mainly near the grain boundaries in the latter due to the constraint from the grain boundaries, which is close to the CDRX mechanisms shown in Figs. 12 and 13. Second, the final crystallographic texture, which is not covered in the GM model [4], was implemented in the Toth et al. model [215] showing quantitative agreement with experimental texture evolution results. Third, the Toth et al. model was developed and validated based on experimental observations of ECAP at room temperature with relatively small strains, while the GM model is on the principle designed for large hot deformation. Lastly, the Toth et al. model is a polycrystal plasticity model and will be limited by the available computational capacity when the grain refinement multiplies, while the GM model is a physically based simplified model requiring less computational resources.

It is noted that only a few CDRX models exist in the literature, there is still large room to improve the modelling of CDRX. The formation of microshear bands or kink bands, as discussed in Section 4.2.2, should be considered in any general CDRX model. Solute and second-phase particles, both of which affect grain boundary migration, are for the moment neglected by selecting pure metals. Different mechanisms of CDRX may be involved, i.e., microshear band assisted CDRX and CDRX by progressive increase of misorientation, as experimentally observed for 304-type austenitic stainless steel in Ref [6]. The transition from CDRX to DDRX or co-existence of these two types of recrystallization processes in certain conditions, e.g. for Mg alloys [8], also demands a more versatile and general model.

5. Geometric dynamic recrystallization

5.1. Introduction

While ultra-fine grain structures can be obtained by CDRX through SPD processes like ECAP, HPT, etc., the production is limited to relatively small quantities of material (although recent extensions such as ECAP-Conform [237] improve the production rate). Alternatively, the production of materials for structural application with fine grain size can be realized using conventional techniques such as rolling through GDRX, a concept originated in 1980s by McQueen and co-workers [238–240], in which a new grain structure is formed as a result of change in grain geometry during deformation.

GDRX has been reported in several different materials: high purity Al [241] and commercial purity Al [238,240], Cu [242], pure Zr [20,243, 244], Al—Mg [245,246], AA5083 [247] and AA 6015 alloys [248], Mg—Al—Zn and Mg—Zn—Zr alloys [249,250]. This means GDRX occurs in pure metals, alloys with solute drag, and particle-containing
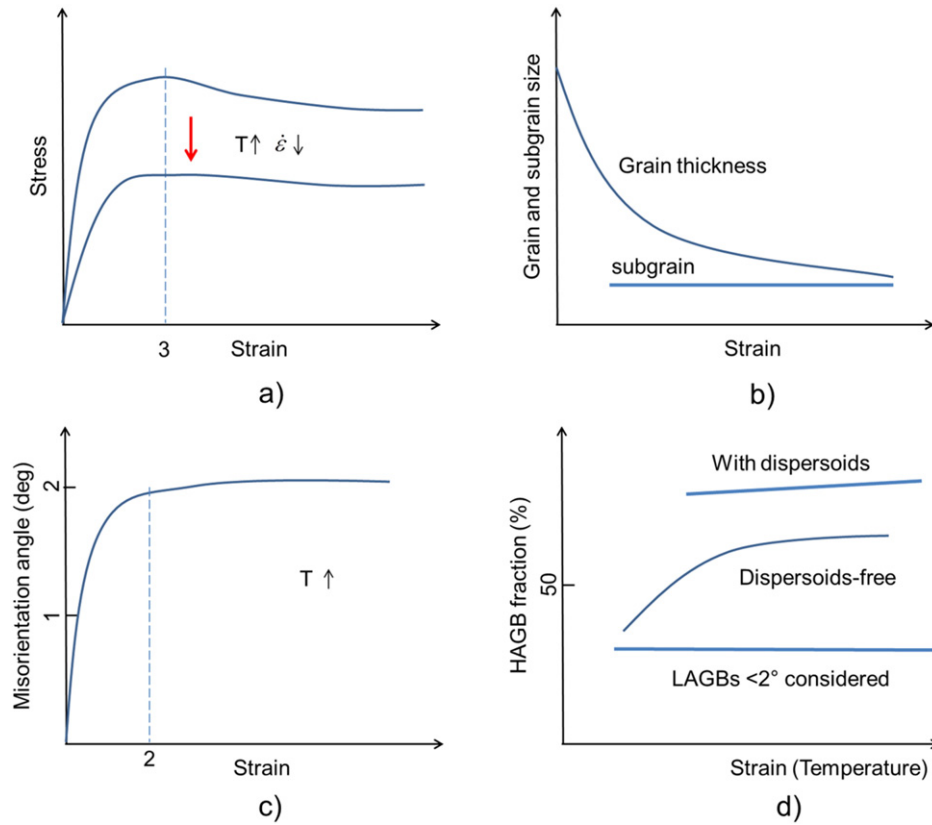
Fig. 20. The evolution of grain thickness (HAGB spacing in the decreasing dimension direction) and subgrain size during GDRX. a) flow stress, noticing the two plateaus, the first one around 1–3, the second one at large strains; b) grain thickness and subgrain size evolution; c) evolution of LAGB misorientation angle measured by TEM (low angles can be detected), deformation bands and HAGB facets are disregarded; d) evolution of HAGBs, where the additional case with LAGBs smaller than 2° is also included for comparison.

alloy systems. GDRX was considered as one type of CDRX by Humpreys and Hatherly [1]. The developments in GDRX was briefly reviewed by Kassner and Barrabes [20], where it was pointed out that it is a general phenomenon that can lead to grain refinement for FCC, BCC and HCP metals. This is why GDRX is treated separately in this review; it is also justified by the fact that GDRX does differ from CDRX in many ways, as will be detailed below.

The main characteristics of GDRX observed from limited amounts of experiments are summarized below:

i) Conditions for GDRX: GDRX is mainly observed for materials with high SFE deformed at elevated temperatures with low strain rates. DRV dominates at low deformation temperatures since the mobility of HAGBs is too low to migrate to form

serrations, while grain growth takes place at very high deformation temperatures [246,247].

ii) Stress-strain curve: the stress initially increases to a relatively broad peak stress, it then declines slowly, possibly due to texture softening, to a steady state at large strains (Fig. 20a) [238–240,251,252].

iii) Subgrain size: subgrains are formed after a critical deformation, first near original HAGBs [245], and the subgrains remain approximately equiaxed and constant in size (Fig. 20b). The steady state subgrain size decreases with increasing Zener-Hollomon parameter [244, 246,251].

iv) Subgrain misorientation: different from CDRX, the misorientation angle of boundaries formed by dislocation reaction saturate at ~2° (see Fig. 20c), which is measured from TEM patterns. Deformation bands usually form with coarse initial grain size, and the facets on
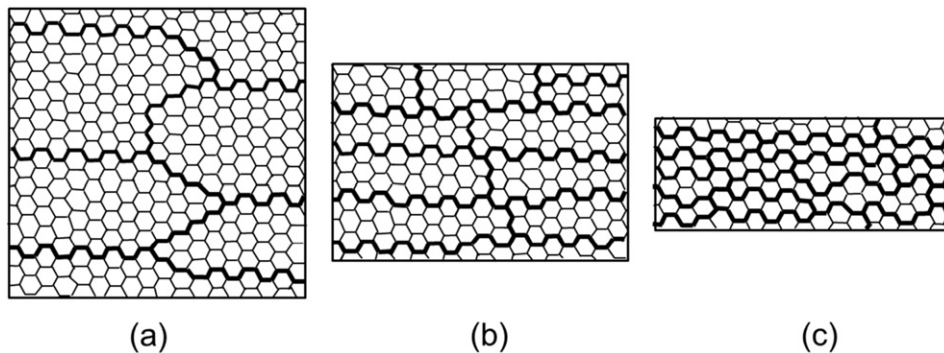

Fig. 21. Schematic graph showing the progress of GDRX. (a) at small deformation, the grain boundaries flatten with well-defined substructure in the matrix; (b) as deformation progresses, the serrated HAGBs (thick lines) become closer, although the subgrain size remains approximately constant; (c) eventually the HAGBs impinge, resulting in a microstructure of mainly HAGBs.

the original HAGBs are disregarded for the computation of the (low) average misorientation in subgrains. Therefore, there is always a bi-modal distribution of misorientation angle during GDRX if all of the grain boundaries are considered [245].

v) HAGB fraction: the literature results on the HAGB fraction during GDRX are confusing. On the one hand, it was reported that there is, depending on the initial grain size, only less than one-sixth to one-third of the subgrain facets in a subgrain belongs to original HAGBs, i.e., they are not the result of CDRX or DDRX [239]. On the other hand, the HAGB fraction is shown to increase with strain and deformation temperature and can reach more than ~80% [244,246]. In the later case, misorientations of <1.5 or 2° were ignored (with the EBSD technique), which might be part of the reason for the large HAGB fraction.

vi) Crystallographic texture: unlike DDRX, the recrystallization texture during GDRX remains largely unchanged, e.g., strong rolling texture during hot rolling, since only little HAGB migration is involved [246]. The texture softening is nevertheless considered as responsible for the stress reduction after the first peak [239,240], see Fig. 20a.

vii) Effect of solute and fine particles: when solute drag and/or particle pinning are involved, the critical strain for subgrain formation and the HAGB fraction increase (Fig. 20d), but the steady state subgrain size decreases, which also means large deformation is required to complete GDRX [240,246].

5.2. Mechanisms

GDRX has been described as the formation of equiaxed grains during hot deformation by (i) the migration of HAGBs to form serrations, (ii) thinning of the grain thickness, and (iii) impingement of serrated HAGBs when approaching 1–2 subgrain size distance (Fig. 20b). As compared to the other two DRX processes, the mechanism of GDRX is relatively simple, and it is explained as follows.

GDRX was commonly formed on deformation of aluminium and its alloys to large strains at elevated temperatures, and is schematically presented in Fig. 21. In these cases, serrations are developed during hot deformation by DRV, with a wavelength similar to the subgrain size, see Fig. 21a. If the material is subjected to a large deformation, significant grain elongation and thinning takes place, which leads to a dramatic increase of grain boundary area, as shown in Fig. 21b. During rolling, for instance, Eq (4) is established to relate the grain thickness in the normal direction (H) as a function of the strain (ε). After a small deformation, the subgrain size during high temperature deformation reaches the steady state value and becomes almost independent of strain. Meanwhile, the grain thickness decreases continuously with deformation, and eventually the size of the boundary serrations will become comparable with the grain thickness with strain approaching 5–10 [20], as illustrated in Fig. 21c. Still referring to Eq. (4), and replacing the thickness of elongated grains (H) by the subgrain size (δ), this critical compressive strain can be calculated as:

$$\varepsilon_{cr}^{GDRX} = \ln\left(\frac{K_1 D_0}{\delta}\right) \tag{20}$$

where K_1 is a constant of the order of unity, it can be adjusted to consider the grain subdivision during deformation [253], i.e. a decreasing D_0. At this stage, "pinching off" may occur by the interpenetration of the serrated boundaries, resulting in a microstructure of small equiaxed grains with a size comparable to the subgrain size. Even though the GDRX process, for simplification purpose, is discussed based on hot rolling, it should be pointed out that similar calculations can be made
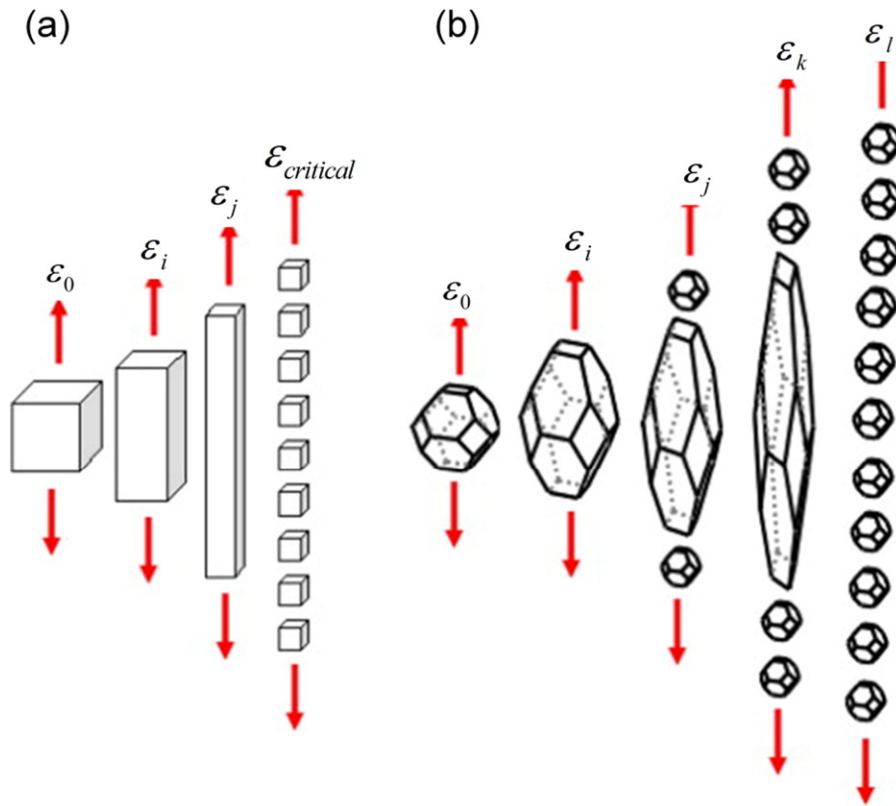
Fig. 22. (a) A representation of grain deformation with the "cubic" GDRX model. GDRX does not begin until $\varepsilon_{critical}$. This produces instantaneous recrystallization. (b) A GDRX modeled with a truncated octahedron (TO). GDRX progresses gradually with strain as both ends of the grain fall within a critical width earlier than other portions. The close packing of subgrains within the grain is also modeled as TOs (Reproduced with permission from Elsevier [5]).

for other processes as well. For instance, it was shown that during hot torsion, the critical strain is [251]:

$$\varepsilon_{cr}^{GDRX} = \frac{D_0}{2\sqrt{3} \cdot \delta} \qquad (21)$$

It follows that the GDRX mechanism mentioned above is only based on geometrical considerations, i.e., the evolution of microstructure is only dependent on the initial grain size and the strain. In fact, there are at least three other aspects that need to be considered during hot deformation.

First, the evolution of grain morphology should be taken into account. One essential condition for the occurrence of GDRX is the formation of serrations at the HAGBs, which is not considered by simply considering the cubic or spherical grain shape. Let us now look at the formation of serration in a more detailed way. During hot deformation, subgrain boundaries first develop near original HAGBs at small strains [245]. The serrations are formed, on both sides of the HAGBs, by local migration of HAGBs at the junctions with the subgrain boundaries formed by DRV. Two types of 2-D models have been used to predict this migration of HAGBs by Martorano and Padilha [254]. Subgrain structures then form at large strains even within the grain interior continuously until the thickness of the HAGBs is reduced to 1–2 subgrain size distance where adjacent grain boundaries may pinch off, leaving an approximately equiaxed microstructure. There is no experimental proof supporting that GDRX can instantaneously complete once the critical strain is reached. This is because the thickness of the deformed grains is not uniform, i.e., some parts of the grain reach the critical strain faster, leading to a gradual transformation of GDRX.

Second, HAGB migration should be considered. If there is no HAGB migration, a fibrous grain structure with elongated subgrain structure instead of close to equiaxed subgrain structure will form after the critical strain calculated from (20), which is essentially a highly deformed microstructure [246ff]. The driving force for HAGB migration, with the aim of reducing the density of HAGBs, is due to boundary curvature. The migration of HAGBs not only changes the grain morphology, it also sweeps the subgrain structure behind the moving boundary. At very high deformation temperatures, HAGB migration may become significant leading to clear dynamic grain growth [251]. Large deformation is then required to reach the critical strain for GDRX.

Third, the introduction of new HAGBs either by grain subdivision or transformed LAGB may not be ignored. Grain subdivision [253] is most significant during the earlier stages of deformation, but little subdivision occurs in Al alloys with average grain size less than ~15 μm [255]. High deformation temperature also favours homogenous deformation, i.e., reduced grain subdivision. The transformation of LAGBs into HAGBs during hot deformation, either by the formation of deformation/shear bands [18] or the progressive increasing of LAGB misorientations [4], has been discussed when treating CDRX in Section 4. More HAGBs will accelerate the GDRX process by reducing the average HAGB (grain) thickness.

5.3. Numerical models

Although the mechanisms of GDRX are generally well understood and have been experimentally observed in different metals and alloys, the attempts to model this process are mostly based on geometrical considerations using cubic or spherical grain shapes. This in general
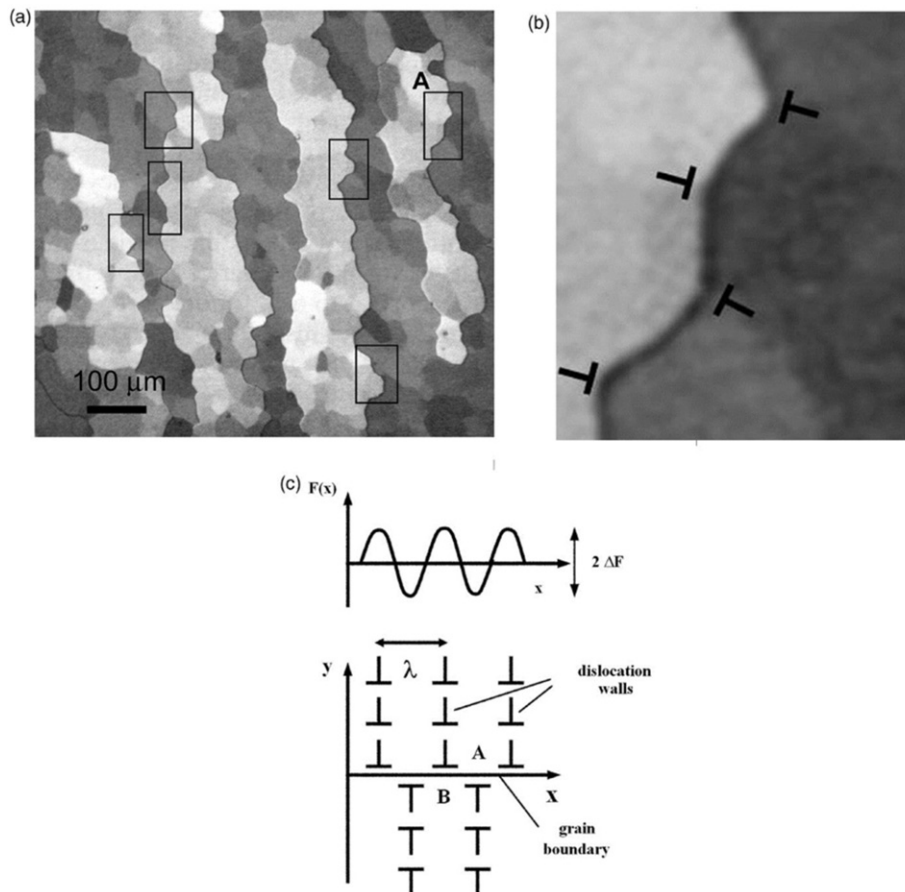
Fig. 23. Explanation of the adopted physical model: (a) optical micrograph of high-purity aluminium revealed in polarized light during GDRX (adapted from Kassner [257]); (b) Enlarged image of region A; (c) physical model of a high-angle boundary between grains A and B, within which dislocation walls separated by interspacing λ cause a driving pressure F that varies sinusoidally with amplitude ΔF and zero mean value (Reprinted by permission of Taylor & Francis Ltd [254]).

qualitatively predicts well the microstructure evolution [5,246,251, 256]. In addition to the geometrical change due to imposed strain, grain morphology evolution, HAGB migration and the introduction of new HAGBs also affect the GDRX process during deformation at elevated temperatures. Even though several GDRX models have been proposed to improve the oversimplified GDRX model that is based purely on geometrical consideration, it seems none of them has fully taken into account all these aspects. In what follows, the attempts to consider for grain morphology evolution [5,254] and HAGB migration [251] are summarized.

5.3.1. The De Pari et al. model

If GDRX only depends on the initial grain size and deformation strain, as predicted by Eqs. (20) or (21), the microstructure will instantaneously be transformed into an equiaxed grain structure when the critical strain is reached. However, experimental evidence has clearly shown that this process takes place gradually [244–246,251]. Considering the limitation of using cubic or spherical grains, De Pari et al. [5] proposed a GDRX model using a 14-sided, three-dimensional truncated octahedron (TO), as shown in Fig. 22. The surface of this TO is comprised of eight hexagons and six squares, one essential advantage of using this shape is its space-filling feature.

During deformation, work hardening and DRV take place, and a substructure with LAGBs is developed. The subgrains are assumed to be equiaxed and equal-sized regardless of the strain, the size is only dependent on the stress. The original TO changes its shape during deformation, the thickness of HAGBs decreases, but the narrow edges thin faster than the bulk of the TO. The subgrains at the edges of both ends pinch off when the critical strain is reached, this process continues until the entire TO has narrowed down to the critical width for GDRX. The result is thus a gradual transformation of GDRX, instead of the instantaneous one if cubic grain shape is assumed, as shown in Fig. 22a.

However, this GDRX model is still of pure geometrical nature. The occurrence of serrations is not explicitly included in the model. The evolution of HAGB spacing other than geometrical consideration is also not elucidated.

5.3.2. The Martorano and Padilha model

Even though a more realistic grain shape is considered in the De Pari et al. model [5], the HAGB migration is not considered there. The original grain boundary is initially flat before deformation. When deformation is applied, as discussed earlier, dislocation walls (subgrain boundaries) are first formed on both sides of the original HAGBs. These HAGBs thus are subjected to a driving pressure F caused by the subgrain boundaries inside the adjacent grains, leading to the formation of serrations, as shown in Fig.23. Martorano and Padilha [254] quantified the driving pressureF, assuming that F varies sinusoidally along the boundary as follows

$$F = \Delta F \sin \frac{2\pi x}{\lambda} \tag{22}$$

Where$x$ is the coordinate along the boundary, ΔF is amplitude, and λ the wavelength i.e. the separation distance between dislocation walls.

The local HAGB curvature also provides part of the driving force for HAGBs migration, so the local normal velocity of the boundary (v_n) is

$$v_n = m\left(\frac{\gamma_{GB}}{R} + F\right) \tag{23}$$

where m is the boundary mobility, R the local radius of curvature of the HAGB, and γ_{GB} the boundary energy per unit area. The migration of the 2-D boundary was described as$y = y(x,t)$, where t is time. The normal velocity can be calculated as

$$v_n = (\partial y/\partial t)\left(1 + \dot{y}^2\right)^{-1/2} \tag{24}$$

where $\partial y/\partial t$ is the boundary velocity in the y direction and $(1 + \dot{y}^2)^{-1/2}$ is the magnitude of the component of the boundary normal in the y direction. The radius of curvature (R) can also be easily found through:

$$R = \frac{\left(1 + \dot{y}^2\right)^{3/2}}{\ddot{y}} \tag{25}$$

Combining these equations yields a differential equation relating the evolution of y with x and t, which can be solved numerically by the finite difference method with appropriate initial conditions, or using a so called least square-normal and curvature model. The interested readers are directed to Ref [254] for more details.

Due to the lack of experimental data on subgrain structure, the model was not directly validated with experiment. In fact, this model did not even consider the decrease of grain thickness due to deformation, so it is not considered as a complete GDRX model. But this model does predict that boundary becomes serrated with peak and valleys migrating into the two adjacent grains, which is a necessary condition for the occurrence of GDRX. Further investigation should focus on changing deformation temperature, strain rate and composition of the investigated materials. Geometric shape change due to the imposed strain and grain refinement or break up [252,253] during hot deformation should also be considered.

5.3.3. The Pettersen et al. model

The geometric shape change due to imposed strain in hot torsion was considered by Pettersen et al. [252]. Simple calculation leads to the evolution of the HAGB thickness evolution by assuming a cubic grain shape:

$$D = \frac{D_0}{\sqrt{1 + 3\varepsilon^2}} \tag{26}$$

where D_0 is the grain thickness before deformation and ε is the true strain. The critical strain is then obtained by replacing the average HAGB thickness D with the subgrain size δ, and this has been previously shown already in Eq. (21). In addition to this geometric shape change, Pettersen et al. also considered (i) the grain breakup, which leads to the *decrease* of D during deformation, and (ii) dynamic grain growth associated with the *increase* of D observed during their experiments.

The grain size evolution is calculated using the following differential equation that is composed of two parts:

$$\frac{dD}{d\varepsilon} = \frac{dD^+}{d\varepsilon} + \frac{dD^-}{d\varepsilon} \tag{27}$$

where $dD^+/d\varepsilon$ relates to dynamic grain growth and $dD^-/d\varepsilon$ considers the grain refinement due to both geometric shape changes and HAGB break up. Grain growth is solely driven by boundary curvature forces, hence

$$\frac{dD^+}{dt} = m\left(\frac{4\gamma_{GB}}{D}\right) \tag{28}$$

with grain boundary mobility $m = m_0 \exp(-\frac{Q}{RT})$. Replacing dt by $d\varepsilon/\dot{\varepsilon}$ and combining Eqs. (5) and (28) gives

$$\frac{dD^+}{d\varepsilon} = \frac{4\gamma_{GB}m_0}{ZD} \tag{29}$$

Since there is currently no developed theory to predict the grain refinement in quantitative or analytical manners, the grain refinement is calculated in an empirical way using the assumption that the grain shape change observed in the particle-containing AA6082 alloy are

nearly athermal in nature, i.e., restoration reactions are inhibited by the Zener pinning effect:

$$\frac{dD^-}{d\varepsilon} = \left[1 - \left(\frac{1}{4}\varepsilon + 1\right) exp(-2\varepsilon)\right] \cdot nAD\left(\frac{D}{D_0}\right)^{1/n} \tag{30}$$

where $A = 278$, and $n = 0.5$.

By combining Eqs. (27), (29) and (30), the evolution in grain thickness can be obtained at any strain rate and temperature (Zener-Hollomon parameter), which was proven to be much better than just considering geometrical shape changing using Eq. (26). This model, however, did not consider the non-uniform grain shape as suggested in the De Pari et al. model [5] nor the formation of serrations at HAGBs that is considered by Martorano and Padilha [254]. Dynamic grain growth can also be induced by the local dislocation density differences [258], besides the capillarity effects.

5.3.4. Summary

As compared to DDRX and CDRX models, the few GDRX models found in the literature are generally over simplified. First, most of them just focus on the geometric shape change due to the imposed strain, which is actually only valid before the critical strain necessary to pinch off the grains, after which the HAGB thickness does not reduce anymore. Second, these models in general cannot predict the stress-strain curve, which is always of industrial interest. One reason is that the dislocation density evolution which can be used to estimate flow stress was not considered in these models. The fact that a stress-strain curve is difficult to obtain during experiments such as hot rolling might be another reason. Third, the grain morphology, which might be not so important for DDRX and CDRX but is of particular importance to GDRX, has never been fully taken into account. This includes the combined effect of the formation of serrations and the non-uniform grain shape. Fourth, HAGB migration due to grain break up and/or dynamic grain growth might become important in specific conditions, and thus need to be considered for any general GDRX models aiming for good predictions at different thermal mechanical conditions. Last, the quantitative effects of solutes and second phase particles on GDRX that are usually present in commercial alloys, are generally neglected in these models.

6. Summary and perspectives

6.1. Summary

The three DRX processes, i.e., DDRX, CDRX and GDRX, occurring in different TMP conditions *at high temperatures* for various metallic materials have been reviewed. The terminologies used in DRX field were summarized, together with the key factors influencing the DRX processes, and the experimental techniques to characterize them. An emphasis was given on the mechanisms and the existing numerical models.

DDRX, also known as conventional DRX, is obviously the most extensively studied DRX process. DDRX operates in low to medium SFE materials at high temperatures ($T > 0.5$ Tm). At this stage, it is generally accepted that DDRX mainly initiates by strain induced bulging of original grain boundaries and a necklace structure which is composed of fine equiaxed recrystallized grains is formed. DDRX may also occur at or near other heterogeneous sites such as shear bands, kink bands, but these sites are more frequently produced at low deformation temperature or high strain rates [259–261]. It is also evident that the new grains may be formed by twinning at high strain levels, a fact that is not well considered so far in the existing numerical models. In general, the steady state of DDRX in terms of flow stress, recrystallized grain size as a function of deformation temperature and deformation strain rate is well established. The DDRX at varying TMP conditions, however, needs further investigation. This is because it is clear from experiments that different DRX mechanisms can act together or in sequence with

changing TMP. It becomes even more complex if precipitation, which affects nucleation of recrystallization as well as grain boundary migration, takes place concurrently with deformation. There exist a large number of numerical models of DDRX, most of them work well in some selected conditions. However, none of these models is deemed as a general model that takes all key ingredients of DDRX into account and is able to model DDRX in varying conditions for particle-containing materials.

In terms of CDRX, it was found that this DRX process takes place in all metals and alloys irrespective of their SFE when the deformation temperature is relatively low ($T < 0.5$ Tm), by severe plastic deformation. At high temperatures, however, CDRX is most frequently observed in high SFE materials. The mechanism of CDRX is not as well understood as for DDRX, the key issue is how the LAGBs increase their misorientation and transform into HAGBs. At low deformation temperatures, it appears that LAGBs can increase their misorientation homogeneously but the misorientation saturates at relatively low values, and it is the formation of microshear bands or kink bands that eventually leads to the formation of HAGBs. At high deformation temperatures, microshear bands or kink bands become less significant, the transformation of LAGBs to HAGBs is done either by the homogeneous increase of misorientation or progressive lattice rotation near grain boundaries. Many experimental observations pointed out that the formation of HAGBs also depends on the grain orientations [222], and there exist some stable orientations, in which the increase in misorientation is not sufficient to form new HAGBs even at large deformations [213,214]. A complete systematic study on CDRX by varying initial grain sizes, grain orientations, chemical compositions, deformation temperatures and strain rates etc., providing quantitative data on flow stress, crystal size and misorientation evolutions, is still missing. CDRX in more complex situations where precipitation or fine second-phase particles are involved, or in varying TMP conditions, also needs further exploitation. In terms of numerical modelling, only a sparse number of CDRX models are found in the literature. This is partly due to the lack of a clear image on the CDRX process mechanisms.

As compared to the two DRX processes mentioned above, GDRX appears quite simple. The geometric shape change due to deformation was studied under different deformation modes such as hot rolling, hot torsion and plane strain compression. It is concluded that GDRX takes place once the thickness of the HAGBs reaches 1–2 subgrain size distance. This often means, even it is not explicitly stated, that GDRX occurs simultaneously for each grain. Since the occurrence of GDRX is very much dependent on the thickness of HAGBs, the grain morphology is of greater importance as compared to DDRX and CDRX. This includes the local variations such as serrations, as well as the global shape, i.e., spherical, cubic or any other shapes. HAGB migration due to dislocation density difference or grain boundary energy, and the introduction of new HAGBs, also need to be considered to explain the discrepancies experimentally observed in terms of the evolution of the thickness of HAGBs. Similarly to the other two DRX processes, precipitation or fine second-phase particles affect the GDRX process through retarding grain boundary migration. Different models are developed, and at this stage, physically based models combining the overall geometric shape change with the local grain morphology (serrations) and HAGB migration, as well as the formation of new HAGBs are still missing. Since most of the above mentioned phenomena are already modeled, it seems realistic to combine them into a single model.

In summary, it can be said that although some of the aspects related to DRX still need further investigation (which will be detailed below), the existing knowledge obtained from both experiments and simulations can already provide valuable help on controlling the microstructure evolution during thermomechanical processing.

6.2. Topics for further investigation

Although DRX processes are of great industrial importance, they are far from being well understood. Part of the reason is related to the

difficulties in experimental studies such as (i) the presence of temperature gradients in the sample (at high temperature) which leads to strain localization, (ii) the heterogeneous nucleation sites within the deformed matrix, (iii) the requirement of fast quenching to prevent SRX or PDRX after termination of deformation and also possible phase transformations, (iv) the difficulties for conducting in-situ analysis with electron microscopy etc. These issues also hinder the development of more advanced DRX models, in which an appropriate nucleation law is essential. The better understanding of nucleation phenomenon, which is by no means homogenous, requires to overcome many technical difficulties, including these described above. Some important aspects that are worth further investigations are listed below:

1) On the action of different DRX mechanisms. There are clear evidences that different DRX mechanisms can act together or in sequence. For instance, the co-existence of DDRX and CDRX was reported in AZ31 [8], while it is suggested that CDRX and GDRX can also act together [5] in AA6061 during hot rolling. The change of restoration mechanisms during deformation was reported when varying initial grain size, material purity, grain orientation and deformation temperatures [6,11,12,40,262–266]. It is now time to ask why the change of DRX mechanism occurs and whether this can be modelled numerically.

2) On the ambiguity between CDRX and GDRX. Due to the existing similarities and differences between CDRX and GDRX, careful experiments should be performed in appropriate deformation conditions to further investigate the distinction between them. One possible way is to deform materials with large initial grain sizes, such that transformation of LAGB into HAGB through CDRX is done before the HAGB thickness reduces to 1–2 subgrain sizes.

3) On the development of DRX. While the initiation of DRX has usually been carefully characterized and modelled, less attention has been paid to the development of DRX afterwards. It has been realized that nucleation can occur at large strains through the formation of twins during DDRX, while the formation of mircoshearbands may contribute to the formation of HAGBs in CDRX. However, more investigations are clearly needed on these mechanisms such as their dependence on material types, deformation temperature and strain rate.

4) On the heterogeneous nucleation sites within the deformed microstructure. Another clear direction that needs further investigation is related to the effect of heterogeneous nucleation sites such as kink band [267] and (micro)shear bands [268] on nucleation of DRX. It is equally important to identify how and when these heterogeneous sites are created, as well as the important factors that affect the formation of these sites.

5) On the effect of second-phase particles. The evolution of second-phase particles during DRX by dynamic precipitation or dissolution makes the quantitative analysis of these particles effects very complex. While the retarding effect of fine second-phase particles on HAGB is generally considered by the Zener pinning theory according to their average size and volume fraction, there is evidence that this retarding effect is also dependent on their spatial distribution, coherency with the matrix, shape and nature of the retarded grain boundary. It is of great interest to be able to use second-phase particles to control the final grain size and crystallographic texture through DRX.

6) On varying deformation conditions. Driven by the industrial demands, there is a need to study DRX in varying deformation conditions that are close to industrial practice. The microstructure evolution under these conditions is more complex than in constant conditions, change of DRX mechanisms can occur, and the instantaneous microstructure also depends on deformation history. In terms of numerical modelling, one state variable is not enough for modelling DRX in variable conditions, e.g., deformation with abrupt change of strain rate and temperature, since it does not account for the short-scale transient behaviour [269,270].

7) On the advanced characterization of DRX. The in-situ characterization of grain boundary mobility and nucleation behavior in 3-D will significantly improve our current understanding on DRX and thus help us to build advanced numerical models. Integrating different characterization techniques together to provide complementary sets of data on DRX should be another important direction in this regard.

8) On the construction of DRX processing maps. Processing maps [271] can be used to design hot working schedules in a wide range of materials. However, DRX depends on many different factors such as deformation temperature and strain rate, deformation strain, initial grain size, SFE etc. It is therefore worth building 2D ($\dot{\varepsilon}$,T) processing maps considering important affecting factors, based on the large amount of existing literature data.

References

[1] F.J. Humphreys, M. Hatherly, Recrystallization and Related Annealing Phenomena, 2nd edn. Elsevier, Oxford, 2004.
[2] H.J. McQueen, Mater. Sci. Eng. A 387-389 (2004) 203–208.
[3] D.G. Cram, H.S. Zurob, Y.J.M. Brechet, C.R. Hutchinson, Acta Mater. 57 (2009) 5218–5228.
[4] S. Gourdet, F. Montheillet, Acta Mater. 51 (2003) 2685–2699.
[5] L. De Pari, W.Z. Misiolek, Acta Mater. 56 (2008) 6174–6185.
[6] Z. Yanushkevich, A. Belyakov, R. Kaibyshev, Acta Mater. 82 (2015) 244–254.
[7] H. Yamagata, Y. Ohuchida, N. Saito, M. Otsuka, Scr. Mater. 45 (2001) 1055–1061.
[8] A.G. Beer, M.R. Barnett, Metall. Mater. Trans. A 38A (2007) 1856–1867.
[9] P. Cizek, Acta Mater. 106 (2016) 129–143.
[10] D.T. Pierce, J.A. Jimenez, J. Bentley, D. Raabe, J.E. Wittig, Acta Mater. 100 (2015) 178–190.
[11] A. Galiyev, R. Kaibyshev, G. Gottstein, Acta Mater. 49 (2001) 1199–1207.
[12] A. Dehghan-Manshadi, P.D. Hodgson, Metall. Mater. Trans. A 39A (2008) 2830–2840.
[13] C. Chauvy, P. Barberis, F. Montheillet, Mater. Sci. Eng. A 431 (2006) 59–67.
[14] K. Wang, G. Liu, J. Zhao, J. Wang, S. Yuan, Mater. Des. 91 (2016) 269–277.
[15] X. Fan, Z. He, P. Lin, S. Yuan, Mater. Des. 94 (2016) 449–456.
[16] H.J. McQueen, M.E. Kassner, Scr. Mater. 51 (2004) 461–465.
[17] R.D. Doherty, D.A. Hughes, F.J. Humpheys, J.J. Jonas, D. Juul Jensen, M.E. Kassner, W.E. King, T.R. McNelley, H.J. McQueen, A.D. Rollett, Mater. Sci. Eng. A 238 (1997) 219–274.
[18] T. Sakai, A. Belyakov, R. Kaibyshev, H. Miura, J.J. Jonas, Prog. Mater. Sci. 60 (2014) 130–207.
[19] A.L. Etter, T. Baudin, N. Fredj, R. Penelle, Mater. Sci. Eng. A 445-446 (2007) 94–99.
[20] M.E. Kassner, S.R. Barrabes, Mater. Sci. Eng. A 410-411 (2005) 152–155.
[21] W.H. Van Geertruyden, W.Z. Misiolek, P.T. Wang, Mater. Sci. Eng. A 419 (2006) 105–114.
[22] P.A. Beck, P.R. Sperry, J. Appl. Phys. 21 (1950) 150–152.
[23] I.L. Dillamore, C.J.E. Smith, T.W. Watson, Met. Sci. J. 1 (1967) 49–54.
[24] P. Faivre, R.D. Doherty, J. Mater. Sci. 14 (1979) 897–919.
[25] A.R. Jones, B. Ralph, N. Hansen, Proc. R. Soc. A368 (1979) 345–357.
[26] R.D. Doherty, J. Szpunar, Acta Metall. 32 (1984) 1789–1798.
[27] J.E. Bailey, P.B. Hirsch, Proc. R. Soc. Lond. A 267 (1962) 11–30.
[28] R.E. Smallman, A.H.W. Ngan, Physical Metallurgy and Advanced Materials Engineering, Elsevier, Oxford, U.K, 2007.
[29] A.W. Ruff, Metall. Trans. 1 (1970) 2391–2413.
[30] P.C.J. Gallagher, Metall. Trans. 1 (1970) 2429–2461.
[31] B. Mahato, S.K. Shee, T. Sahu, S. Ghosh Chowdhury, P. Sahu, D.A. Porter, L.P. Karjalainen, Acta Mater. 86 (2015) 69–79.
[32] C.C. Bampton, I.P. Jones, M.H. Loretto, Acta Metall. 26 (1978) 39–51.
[33] T. Ericsson, Acta Metall. 14 (1966) 853–865.
[34] S.L. Shang, C.L. Zacherl, H.Z. Fang, Y. Wang, Y. Du, Z.K. Liu, J. Phys. Condens. Matter 24 (2012) 505403.
[35] L.E. Murr, Interfacial Phenomena in Metals and Alloys, Addison-wesley, Reading, 1975.
[36] H. Conard, J. Narayan, Scr. Mater. 42 (2000) 1025–1030.
[37] J.P. Sah, G.J. Richardson, C.M. Sellars, Met. Sci. 8 (1974) 325–331.
[38] M.E.I. Wahabi, L. Gavard, F. Montheillet, J.M. Cabrera, J.M. Prado, Acta Mater. 53 (2005) 4605–4612.
[39] T. Sakai, J.J. Jonas, Acta Metall. 32 (1984) 189–209.
[40] A. Belyakov, K. Tsuzaki, H. Miura, T. Sakai, Acta Mater. 51 (2003) 847–861.
[41] X. Yang, M. Sanada, H. Miura, T. Sakai, Mater. Sci. Forum 488-489 (2005) 223–226.
[42] W.X. Wu, L. Jin, J. Dong, Z.Y. Zhang, W.J. Ding, Mater. Sci. Eng. A 556 (2012) 519–525.

[43] H. Hallberg, M. Wallin, M. Ristinmaa, Mater. Sci. Eng. A 527 (2010) 1126–1134.
[44] Y. Takigawa, M. Honda, T. Uesugi, K. Higashi, Mater. Trans. 49 (2008) 1979–1982.
[45] J. Gil Sevillano, P. van Houtte, E. Aernoudt, Prog. Mater. Sci. 25 (1980) 69–134.
[46] E. Nes, Prog. Mater. Sci. 41 (1998) 129–193.
[47] C.M. Sellars, W.J. Tegart, Int. Metall. Rev. 17 (1972) 1–24.
[48] O. Sitdikov, T. Sakai, A. Goloborodko, H. Miura, R. Kaibyshev, Philos. Mag. 85 (2005) 1159–1175.
[49] H.J. McQueen, O. Knustad, N. Ryum, J.K. Solberg, Scr. Metall. 19 (1985) 73–78.
[50] B. Derby, M.F. Ashby, Scr. Metall. 21 (1987) 879–884.
[51] B. Derby, Acta Metall. Mater. 39 (1991) 955–962.
[52] S.E. Ion, F.J. Humphreys, S. White, Acta Metall. 30 (1982) 1909–1919.
[53] A. Dehghan-Manshadi, The Evolution of Recrystallization During and Following Hot Deformation, Deakin University, 2007 (Ph. D thesis).
[54] K. Huang, Towards the Modelling of Recrystallization Phenomena in Multi-pass Conditions: Application to 304 L Steel, École Nationale Supérieure des Mines de Paris, 2011 (Ph. D thesis).
[55] T. Sakai, H. Miura, Mater. Sci. Forum 706–709 (2012) 1829–1834.
[56] M. Sanjari, S.A. Farzadfar, I.H. Jung, E. Essadiqi, S. Yue, Mater. Sci. Technol. 28 (2012) 437–447.
[57] O. Sitdikov, R. Kaibyshev, Mater. Trans. 42 (2001) 1928–1937.
[58] Q. Guo, D. Li, H. Peng, S. Guo, J. Hu, P. Du, Rare Metals 31 (2012) 215–220.
[59] S. Mandal, M. Jayalakshmi, A.K. Bhaduri, V. Subramanya Sarma, Mater. Metall. Trans. A 45 (2014) 5645–5656.
[60] G.C. Cornfield, R.H. Johnson, J. Iron Steel Inst. 211 (1973) 567–573.
[61] J.J. Urcola, C.M. Sellars, Acta Metall. 35 (1987) 2637–2647.
[62] J.J. Urcola, C.M. Sellars, Acta Metall. 35 (1987) 2649–2657.
[63] J.J. Urcola, C.M. Sellars, Acta Metall. 35 (1987) 2659–2669.
[64] G.J. Baxter, T. Furu, Q. Zhu, J.A. Whiteman, C.M. Sellars, Acta Mater. 47 (1999) 2367–2376.
[65] T. Furu, H.R. Shercliff, G.J. Baxter, C.M. Sellars, Acta Mater. 47 (1999) 2377–2389.
[66] C.M. Sellars, Q. Zhu, Mater. Sci. Eng. A 280 (2000) 1–7.
[67] M.F. Abbod, C.M. Sellars, A. Tanaka, D.A. Linkens, M. Mahfouf, Mater. Sci. Eng. A 491 (2008) 290–296.
[68] J.-P.A. Immarigeon, J.J. Jonas, Acta Metall. 19 (1971) 1053–1061.
[69] Y. Huang, F.J. Humphreys, Acta Mater. 45 (1997) 4491–4503.
[70] G. Gottstein, S. Deshpande, Mater. Sci. Eng. 94 (1987) 147–154.
[71] E. Nes, N. Ryum, O. Hunderi, Acta Metall. 33 (1985) 11–22.
[72] K. Huang, R.E. Logé, Zener PinningEditor-in-Chief in: S. Hashmi (Ed.), Reference Module in Materials Science and Materials Engineering, Elsevier, Oxford 2016, pp. 1–8.
[73] F.J. Humphreys, P.N. Kalu, Acta Metall. Mater. 35 (1987) 2815–2829.
[74] C.R. Hutchinson, H.S. Zurob, C.W. Sinclair, Y.J.M. Brechet, Scr. Mater. 59 (2008) 635–637.
[75] S.L. Semiatin, D.S. Weaver, P.N. Fagin, M.G. Glavicic, R.L. Goetz, N.D. Frey, et al., Metall. Mater. Trans. A 35 (2004) 679–693.
[76] R.L. Goetz, Scr. Mater. 52 (2005) 851–856.
[77] Y. Wu, H. Liao, J. Yang, K. Zhou, J. Mater. Sci. Technol. 30 (2015) 1271–1277.
[78] M.J. Luton, C.M. Sellars, Acta Metall. 17 (1969) 1033–1043.
[79] R. Le Gall, J.J. Jonas, Acta Mater. 47 (1999) 4365–7374.
[80] W. Gao, A. Belyakov, H. Miura, T. Sakai, Mater. Sci. Eng. A 264 (1999) 233.
[81] S. Vervynckt, K. Verbekena, P. Thibaux, Y. Houbaert, Mater. Sci. Eng. A 528 (2011) 5519–5528.
[82] H.S. Zurob, Effects of Precipitation, Recovery and Recrystallization on the Microstructural Evolution of Microalloyed Austenite, McMaster University, Hamilton, Ont., Canada, 2003 (phD. Thesis).
[83] F. Tancret, E. Galindo-Nava, P.E.J. Rivera-Diaz-Del-Catillo, Mater. Des. 103 (2016) 293–299.
[84] Y.C. Lin, D.-G. He, M.-S. Chen, X.-M. Chen, C.-Y. Zhao, X. Ma, Z.-L. Long, Mater. Des. 97 (2016) 13–24.
[85] J.D. L'ecuyer, G. L'espérance, Acta Metall. 37 (1989) 1023–1031.
[86] S. Ukai, M. Fujiwara, J. Nucl. Mater. 307-311 (2002) 749–757.
[87] J. Hofstetter, S. Rüedi, I. Baumgartner, H. Kilian, B. Mingler, E.P. -Karadenizd, S. Pogatscher, P.J. Uggowitzer, J.F. Löffler, Acta Mater. 98 (2015) 423–432.
[88] S.H. Mousavi Anijdan, S. Yue, Mater. Sci. Eng. A 528 (2011) 803–807.
[89] P.D. Hodgson, R.K. Gibbs, ISIJ Int. 32 (1992) 1329–1338.
[90] B. Dutta, E. Valdes, C.M. Sellars, Acta Metall. Mater. 40 (1992) 653–662.
[91] E.J. Palmiere, C.I. Garcia, A.J. DeArdo, Mater. Metall. Trans. A 25A (1994) 277–286.
[92] I. Nikulin, A. Kipelova, S. Malopheyev, R. Kaibyshev, Acta Mater. 60 (2012) 487–497.
[93] H. Miura, H. Tsukawaki, T. Sakai, J.J. Jonas, Acta Mater. 56 (2008) 4944–4952.
[94] J.-Q. Su, T.W. Nelson, R. Mishra, M. Mahoney, Acta Mater. 51 (2003) 713–729.
[95] D.S. Fields, W.A. Backofen, Proc. Am. Soc. Test Mater. 57 (1957) 1259–1272.
[96] G.E. Dieter, H.A. Kuhn, S.L. Semiatin, Handbook of Workability and Process Design, American Society of Metals, Materials Park, OH, 2003.
[97] S. Khoddam, P.D. Hodgson, J. Mater. Process. Technol. 153-154 (2004) 839–845.
[98] E.I. Poliak, J.J. Jonas, Acta Metall. Mater. 44 (1996) 127–136.
[99] A. Najafizadeh, J.J. Jonas, ISIJ Int. 46 (2006) 1679–1684.
[100] P.L. Orsetti Rossi, C.M. Sellars, Acta Mater. 45 (1996) 137–148.
[101] S.I. Wright, M.M. Nowell, D.P. Field, Microsc. Microanal. 17 (2011) 316–329.
[102] A. Delesse, Procede mechanique Pour determiner la composition des roches, Ann Des Mines, 13, 1848, pp. 379–388 (fourth series).
[103] E.E. Underwood, Quantitative Stereology, Addison-Wesley Publishing Company, 1981.
[104] G.A. Wilber, J.R. Bell, J.H. Bucher, W.J. Childs, Trans. TMS-AIME 244 (1968) 2305–2308.
[105] R.A.P. Djaic, J.J. Jonas, Sta J. Iron Steel Inst. 210 (1972) 256–261.
[106] R.A.P. Djaic, J.J. Jonas, Mettal. Trans. 4 (1973) 621–624.
[107] L.P. Karjalainen, Mater. Sci. Technol. 11 (1995) 557–565.
[108] N. Zaafarani, D. Raabe, R.N. Singh, F. Roters, S. Zaefferer, Acta Mater. 54 (2006) 1863–1876.
[109] W. Xu, M. Ferry, N. Mateescu, J.M. Cairney, F.J. Humphreys, Mater. Charact. 58 (2007) 961–967.
[110] M. Ferry, W.Q. Xu, M.Z. Quadir, N.A. Zinnia, K.J. Laws, N. Mateescu, L. Robin, L. Bassman, J.M. Cairney, J.F. Humphreys, A. Albou, J.H. Driver, Mater. Sci. Forum 715–716 (2012) 41–50.
[111] G.H. Fan, Y.B. Zhang, J.H. Driver, D. Juul Jensen, Scr. Mater. 72-73 (2014) 9–12.
[112] J.L. Urai, S. Zaefferer, D. Raabe, Acta Mater. 54 (2006) 1369–1380.
[113] S. Schmidt, S.F. Nielsen, C. Gundlach, L. Margulies, X. Huang, D.J. Jensen, Science 305 (2004) 229–232.
[114] Y. Yogo, K. Tanaka, K. Nakanishi, Mater. Sci. Forum 638-642 (2010) 1077–1082.
[115] J.L. Urai, F.J. Humphreys, S.E. Burrows, J. Mater. Sci. 15 (1980) 1231–1240.
[116] H. Yamagata, Acta Metall. Mater. 43 (1995) 723–729.
[117] S. Kaboli, P.T. Pinard, J. Su, S. Yue, R. Gauvin, IOP Conf. Series: Materials Science and Engineering, 55, 2014 012007.
[118] M. Peternell, D.S. Russell-Head, C.J.L. Wilson, J. Microsc. 242 (2011) 181–188.
[119] S.I. Wright, M.M. Nowell, in: A.J. Schwartz, M. Kumar, B.L. Adams, D.P. Field (Eds.), Electron Backscatter Diffraction in Materials Science, 2nd ed.Springer, New York 2009, pp. 329–337.
[120] A. Tatschl, O. Kolednik, Mater. Sci. Eng. A 356 (2003) 447–463.
[121] Y. Huang, F.J. Humphreys, I. Brough, J. Microsc. 208 (2002) 18–23.
[122] M.J. Luton, C.M. Sellars, Acta Metall. 17 (1969) 1033–1043.
[123] T. Sakai, J.J. Jonas, Acta Metall. 32 (1984) 189–209.
[124] A. Dehghan-Manshadi, M.R. Barnett, P.D. Hodgson, Metall. Mater. Trans. A 39A (2008) 1359–1370.
[125] L. Blaz, T. Sakai, J.J. Jonas, Met. Sci. 17 (1983) 609–616.
[126] D. Ponge, G. Gottstein, Acta Mater. 46 (1998) 69–80.
[127] M. El Wahabi, L. Gavard, F. Montheillet, J.M. Cabrera, J.M. Prado, Acta Mater. 53 (2005) 4605–4612.
[128] M. Ohashi, T. Endo, T. Sakai, J. Jpn. Inst. Metals 54 (1990) 435–441.
[129] A.I. Fernandez, P. Uranga, B. Lopez, J.M. Rodriguez-Ibabe, Mater. Sci. Eng. A 361 (2003) 367–376.
[130] U.F. Kocks, H. Mecking, Prog. Mater. Sci. 48 (2003) 171–273.
[131] R. Sandström, R. Lagneborg, Acta Metall. 23 (1975) 387–398.
[132] R. Sandström, R. Lagneborg, Scr. Metall. 9 (1975) 59–65.
[133] W. Roberts, B. Ahlblom, Acta Metall. 26 (1978) 801–813.
[134] B. Derby, M.F. Ashby, Scr. Metall. 21 (1987) 879–884.
[135] R. Ding, Z.X. Guo Acta, Mater 49 (2001) 3163–3175.
[136] E.I. Galindo-Nava, J. Sietsma, P.E.J. Rivera-Diaz-del-Catillo, Acta Mater. 60 (2012) 2615–2624.
[137] F. Montheillet, D. Piot, N. Matougui, M.L. Fares, Metall. Mater. Trans. A 45 (2014) 4324–4332.
[138] Y. Estrin, Dislocation-density-related constitutive modeling, in: A.S. Krausz (Ed.), Unified Constitutive Laws of Plastic Deformation, Academic Press, New York, 1996.
[139] D.S. Svyetlichnyy, J. Majta, J. Nowak, Mater. Sci. Eng. A 576 (2013) 140–148.
[140] R.A. Vandermeer, D. Juul Jensen, Interface Sci. 6 (1998) 95–104.
[141] G. Gottstein, S.L. Shvindlerman, Scr. Metall. Mater. 27 (1992) 1521–1526.
[142] R.A. Vandermeer, D. Juul Jensen, E. Woldt, Metall. Mater. Trans. A 28 (1997) 749–754.
[143] Y. Huang, F.J. Humphreys, Acta Mater. 47 (1999) 2259–2268.
[144] G. Gottstein, D.A. Molodov, L.S. Shvindlerman, D.J. Srolovitz, M. Winning, Curr. Opin. Solid State Mater. Sci. 5 (2001) 9–14.
[145] H. Gleiter, Acta Metall. 17 (1969) 853–862.
[146] M. Winning, G. Gottstein, L.S. Shvindlerman, Acta Mater. 50 (2002) 353–363.
[147] C. Rossard, Contribution à l'étude de la déformation plastique à chaud des aciers, Métaux-Corrosion-Industries 35:102–115 (Part 1), 140–153 (Part 2), 190–205 (Part 3), 1960 (PhD Dissertation).
[148] H. Miura, T. Sakai, S. Andiarwanto, J.J. Jonas, Philos. Mag. 85 (2005) 2653–2669.
[149] H. Miura, T. Sakai, H. Hamaji, J.J. Jonas, Scr. Mater. 50 (2004) 65–69.
[150] S.-I. Kim, Y.-C. Yoo, Mater. Sci. Eng. A311 (2001) 108–113.
[151] C. Roucoules, M. Pietrzyk, P.D. Hodgson, Mater. Sci. Eng. A339 (2003) 1–9.
[152] P. Bernard, S. Bag, K. Huang, R.E. Logé, Mater. Sci. Eng. A 528 (2011) 7357–7367.
[153] O. Beltran, K. Huang, R.E. Logé, Comput. Mater. Sci. 102 (2015) 293–303.
[154] H. Miura, H. Aoyama, T. Sakai, J. Jpn. Inst. Metals 58 (1994) 267–275.
[155] A.M. Wusatowska-Sarnek, H. Miura, T. Sakai Mater, Sci. Eng. A323 (2002) 177–186.
[156] M.D. Drury, F.J. Humphreys, Acta Metall. 34 (1986) 2259–2271.
[157] M.A. Charpagne, T. Billot, J.M. Franchet, N. Bozzolo, J. Alloys Compd. 688 (2016) 685–694.
[158] P. Karduck, G. Gottstein, H. Mecking, Acta Mater. 31 (1983) 1525–1636.
[159] E. Brunger, X. Wang, G. Gottstein, Scr. Mater. 38 (1998) 1843–1849.
[160] X. Wang, E. Brunger, G. Gottste, Scr. Mater. 46 (2002) 875–880.
[161] H. Beladi, P. Cizek, P.D. Hodgson, Metall. Mater. Trans. A 40 (2009) 1175.
[162] S.Q. Zhu, H.G. Yan, X.Z. Liao, S.J. Moody, G. Sha, Y.Z. Wu, S.P. Ringer, Acta Mater. 82 (2015) 344–355.
[163] H.J. McQueen, N.D. Ryan, Mater. Sci. Eng. A 322 (2002) 43–63.
[164] Y.C. Lin, X.M. Chen, Mater. Des. 32 (2011) 1733–1759.
[165] F. Siciliano, K. Minami, T.M. Maccagno, J.J. Jonas, ISIJ Int. 36 (1996) 1500–1506.
[166] S.F. Medina, C.A. Hernandez, Acta Mater. 44 (1996) 165–171.
[167] A. Kolmogorov, Bull. Acad. Sci. USSR Ser. Math. 1 (1937) 355–359.
[168] W. Johnson, R. Mehl, Trans. Am. Inst. Min. Metall. Eng. 135 (1939) 416–458.
[169] M. Avrami, Chem. Phys. 7 (1939) 1103–1112.
[170] M. Avrami, J. Chem. Phys. 8 (1940) 212–224.
[171] J.J. Jonas, X. Quelennec, L. Jiang, E. Martin, Acta Mater. 57 (2009) 2748–2756.

[172] F. Montheillet, O. Lurdos, G. Damamme, Acta Mater. 57 (2009) 1602–1612.
[173] H.S. Zurob, Y. Brechet, J. Dunlop, Acta Mater. 54 (2006) 3983–3990.
[174] E.A. Holm, M.A. Miodownik, A.D. Rollett, Acta Mater. 51 (2003) 2701–2716.
[175] D.G. Cram, X.Y. Fang, H.S. Zurob, Y.J.M. Bréchet, C.R. Hutchinson, Acta Mater. 60 (2012) 6390–6404.
[176] M. Zouari, N. Bozzolo, R.E. Logé, Mater. Sci. Eng. A 655 (2016) 408–424.
[177] E.I. Galindo-Nava, P.E.J. Rivera-Díaz-del-Castillo, Int. J. Plast. 47 (2013) 202–221.
[178] E.I. Galindo-Nava, P.E.J. Rivera-Díaz-del-Castillo, Scr. Mater. 72-73 (2014) 1–4.
[179] E.I. Galindo-Nava, C.M.F. Rae, Mater. Sci. Eng. A 636 (2015) 434–445.
[180] L. Bäcke, ISIJ Int. 50 (2010) 239–247.
[181] H.S. Zurob, Y. Brechet, G. Purdy, Acta Mater. 49 (2001) 4183–4193.
[182] H.S. Zurob, C.R. Hutchinson, Y. Brechet, G. Purdy, Acta Mater. 50 (2002) 3075–3092.
[183] A. Moroux, Z.J. Lok, S. van der Zwaag, Mater. Sci. Forum 467-470 (2004) 393–398.
[184] R. Roumina, C.W. Sinclair, Acta Mater. 58 (2010) 111–121.
[185] C. Schafer, V. Mohles, G. Gottstein, Acta Mater. 59 (2011) 6574–6587.
[186] H. Hallberg, B. Svendsen, T. Kayser, M. Ristinmaa, Comput. Mater. Sci. 84 (2014) 327–338.
[187] K. Huang, R.E. Logé, K. Marthinsen, J. Mater. Sci. 51 (2016) 1632–1643.
[188] K. Huang, Y.J. Li, K. Marthinsen, Mater. Charact. 102 (2015) 92–97.
[189] K. Huang, N. Wang, Y.J. Li, K. Marthinsen, Mater. Sci. Eng. A 601 (2014) 86–96.
[190] K. Huang, O. Engler, Y.J. Li, K. Marthinsen, Mater. Sci. Eng. A 628 (2015) 216–222.
[191] G.C. Cornfield, R.H. Johson, J. Iron Steel Inst. 211 (1973) 567.
[192] T. Takaki, A. Yamanaka, Y. Tomita, ISIJ Int. 51 (2011) 1717–1723.
[193] T. Takaki, C. Yoshimoto, A. Yamanaka, Y. Tomita, Int. J. Plast. 52 (2014) 105–116.
[194] H. Li, C. Wu, H. Yang, Int. J. Plast. 51 (2013) 271–291.
[195] M. Pietrzyk, J. Mater. Process. Technol. 125-126 (2002) 53–62.
[196] A.A. Brown, D.J. Bammann, Int. J. Plast. 32-33 (2012) 17–35.
[197] G. Kugler, R. Turk, Acta Mater. 52 (2004) 4659–4668.
[198] H. Hallberg, Metals 1 (2011) 16–48.
[199] H. Hallberg, M. Wallin, M. Ristinmaa Comput. Mater. Sci. 49 (2010) 25–34.
[200] A.D. Rollett, M.J. Luton, D.J. Srolovitz, Acta Metall. Mater. 40 (1992) 43–55.
[201] P. Peczak, Acta Metall. Mater. 43 (1995) 1279–1291.
[202] T. Takaki, Y. Hisakuni, T. Hirouchi, A. Yamanaka, Y. Tomita, Mater. Trans. 49 (2008) 2559–2565.
[203] T. Takaki, Y. Hisakuni, T. Hirouchi, A. Yamanaka, Y. Tomita, Comput. Mater. Sci. 45 (2009) 881–888.
[204] R. Boulais-Sinou, B. Scholtes, D. Pino Muñoz, C. Moussa, I. Poitrault, I. Bobin, A. Montouchet, M. Bernacki, Proceedings of NUMIFORM, 2016.
[205] H. Hallberg, Model. Simul. Mater. Sci. Eng. 21 (8) (2013) 085012.
[206] P. Zhao, T.S.E. Low, Y. Wang, S.R. Niezgoda, Int. J. Plast. 80 (2016) 38–55.
[207] J.J. Jonas, L.S. Tóth, Scr. Met. Mater. 27 (1992) 1575–1580.
[208] L.S. Tóth, J.J. Jonas, Scr. Met. Mater. 27 (1992) 359–363.
[209] A. Hildenbrand, L.S. Tóth, A. Molinari, J. Baczynski, J.J. Jonas, Acta Mater. 47 (1999) 447–460.
[210] H. Miura, T. Sakai, R. Mogawa, G. Gottstein, Scr. Mater. 51 (2004) 671–675.
[211] C. Perdrix, M.Y. Perrin, F. Montheillet, Mem. Sci. Rev. Métal. 78 (1981) 309–320.
[212] F. Montheillet, P. Costa, et al., (Eds.),24ème Colloque de Métallurgie, INSTN, Saclay 1981, pp. 57–70.
[213] S. Gourdet, F. Montheillet, Mater. Sci. Eng. A 283 (2000) 274–288.
[214] O. Sitdikov, T. Sakai, H. Miura, C. Hama, Mater. Sci. Eng. A 516 (2009) 180–188.
[215] L.S. Toth, Y. Estrin, R. Lapovok, C. Gu, Acta Mater. 58 (2010) 1782–1794.
[216] X. Yang, H. Miura, T. Sakai, Mater. Trans. 43 (2002) 2400–2407.
[217] X. Yang, H. Miura, T. Sakai, Mater. Trans. 44 (2003) 197–203.
[218] A. Belyakov, W. Gao, H. Miura, T.Sakai, Metall. Mater. Trans. A 29A (1998) 2957–2965.
[219] R. Kaibyshev, K. Shipilova, F. Musin, Y. Motohashi, Mater. Sci. Eng. A 396 (2005) 341–351.
[220] K. Tsuzaki, X. Huang, T. Maki, Acta Mater. 44 (1996) 4491–4499.
[221] L. Qing, H. Xiaoxu, Y. Mei, Y. Jinfeng, Acta Metall. Mater. 40 (1992) 1753–1762.
[222] W.C. Liu, D. Juul Jensen, J.G. Morris, Acta Mater. 49 (2001) 3347–3367.
[223] S.S. Razavi-Tousi, J.A. Szpunar, Philos. Mag. 95 (2015) 1425–1447.
[224] H.Y. Wang, Z.–.P. Zhang, L. Zhang, C.–.G. Liu, M. Zha, C. Wang, Q.-C. Jiang, Sci. Rep. 5 (2015) 17100.
[225] S.J. Hales, T.R. McNelley, Acta Metall. 36 (1988) 1229–1239.
[226] S.H. White, Phil. Trans. R. Soc. A 283 (1976) 69–86.
[227] B. Escaig, Phys. Status Solidi 28 (1968) 463–474.
[228] A. Couret, D. Caillard, Acta Metall. 33 (1985) 1447–1454.
[229] B. Legrand, Philos. Mag. A 49 (1984) 171–184.
[230] W. Puschl, G. Schoeck, H.O.K. Kirchner, Philos. Mag. A 56 (1987) 533–563.
[231] K.J. Gardner, R. Grimes, Met. Sci. 13 (1979) 216–222.
[232] T. Sakai, X. Yang, H. Miura, Mater. Sci. Eng. A 234-236 (1997) 857–860.
[233] T. Sakai, A. Belyakov, H. Miura, Metall. Mater. Trans. A 39A (2008) 2206–2214.
[234] G. Buffa, L. Fratini, R. Shivpuri, J. Mater. Process. Technol. 191 (2007) 356–359.
[235] M. Bacca, D.R. Hayhurst, R.M. McMeeking, Mech. Mater. 90 (2015) 148–156.
[236] A. Laasraoui, J.J. Jonas, Metall. Trans. A 22 (1991) 1545–1558.
[237] G.J. Raab, R.Z. Valiev, T.C. Lowe, Y.T. Zhu, Mater. Sci. Eng. A382 (2004) 30–34.
[238] H.J. McQueen, J.K. Solberg, N. Ryum, E. Nes, Philos. Mag. A 60 (1989) 473–485.
[239] J.K. Solberg, H.J. McQueen, N. Ryum, E. Nes, Philos. Mag. A 60 (1989) 447–471.
[240] H.J. McQueen, O. Knustad, N. Ryum, J.K. Solberg, Scr. Metall. Mater. 19 (1985) 73–78.
[241] M.E. Kassner, M.E. Mcmahon, Metall. Trans. A 18 (1987) 835–846.
[242] A.M. Wusatowska-Sarnek, H. Miura, T. Sakai, Mater. Sci. Eng. A 323 (2002) 177–186.
[243] M.T. Perez-Prado, S.R. Barrabes, M.E. Kassner, et al., Acta Mater. 53 (2005) 581–591.
[244] L. Jiang, M.T. Pérez-Prado, P.A. Gruber, E. Arzt, O.A. Ruano, M.E. Kassner, Acta Mater. 56 (2008) 1228–1242.
[245] G.A. Henshall, M.E. Kassner, H.J. McQueen, Metall. Trans. A 23 (1992) 881–889.
[246] A. Gholinia, F.J. Humphreys, P.B. Prangnell, Acta Mater. 50 (2002) 4461–4476.
[247] W. Blum, Q. Zhu, R. Merkel, H.J. McQueen, Mater. Sci. Eng. A205 (1996) 23–30.
[248] E.V. Konopleva, H.J. McQueen, E. Evangelista, Mater. Charact. 34 (1995) 251–264.
[249] H.J. McQueen, M.M. Myshlyaev, A. Mwembela, Can. Metall. Q. 42 (2003) 97–112.
[250] M.M. Myshlyaev, H.J. McQueen, A. Mwembela, E.V. Konopleva, Mater. Sci. Eng. A 337 (2002) 121–133.
[251] T. Pettersen, B. Holmedal, E. Nes, Metall. Mater. Trans. A 34A (2003) 2727–2736.
[252] T. Pettersen, B. Holmedal, E. Nes, Metall. Mater. Trans. A 34A (2003) 2737–2744.
[253] D.A. Hughes, N. Hansen, Acta Mater. 45 (1997) 3871–3886.
[254] M.A. Martorano, A.F. Padilha, Philos. Mag. Lett. 88 (2008) 725–734.
[255] F.J. Humphreys, P.B. Prangnell, J.R. Bowen, A. Gholinia, C. Harris, Philos. Trans. R. Soc. Lond. 357A (1999) 1663–1681.
[256] S. Gourdet, E.V. Konopleva, H.J. McQueen, F. Montheillet, Mater. Sci. Forum 217-222 (1996) 441–446.
[257] M.E. Kassner, Metall. Trans. A 20 (1989) 2182–2185.
[258] S. Gourdet, F. Montheillet, Acta Mater. 50 (2002) 2801–2812.
[259] U. Andrade, M.A. Meyers, K.S. Vecchio, A.H. Chokshi, Acta Metall. Mater. 42 (1994) 3183–3195.
[260] J.A. Hines, K.S. Vecchio, Acta Mater. 45 (1997) 635–649.
[261] M.A. Meyers, Y.B. Xu, Q. Xue, M.T. Perez-Prado, T.R. Mcnelley, Acta Mater. 51 (2003) 1307–1325.
[262] H. Jazaeri, F.J. Humphreys, Acta Mater. 52 (2004) 3239–3250.
[263] A. Belyakov, T. Sakai, H. Miura, R. Kaibyshev, K. Tsuzaki, Acta Mater. 50 (2002) 1547–1557.
[264] A. Belyakov, H. Miura, T. Sakai, Scr. Mater. 43 (2000) 21–26.
[265] M.R. Drury, F.J. Humphreys, S.H. White, Phys. Earth Planet. Inter. 40 (1985) 208–222.
[266] K. Tanaka, M. Otsuka, H. Yamagata, Mater. Trans. JIM 40 (1999) 242–247.
[267] P. Karduck, G. Gottstein, H. Mecking, Acta Metall. 31 (1983) 1525–1536.
[268] Y. Xu, H.J. Yang, M.A. Meyers, Scr. Mater. 58 (2008) 691–694.
[269] H. Mecking, U.F. Kocks, Acta Metall. 29 (1981) (1865-1857).
[270] Y. Estrin, H. Mecking, Acta Metall. 32 (1984) 57–70.
[271] Y.V.R.K. Prasad, T. Seshacharyulu, Mater. Sci. Eng. A 243 (1998) 82–88.